A WAVELET-BASED DAMAGE DETECTION ALGORITHM BASED ON BRIDGE ACCELERATION RESPONSE TO A VEHICLE

D. Hester [1] and A. González [1]

[1]School of Architecture, Landscape & Civil Engineering, University College Dublin, Belfield, Dublin 4, Ireland

Abstract

Previous research based on theoretical simulations has shown the potential of the wavelet transform to detect damage in a beam by analysing the time-deflection response due to a constant moving load. However, its application to identify damage from the response of a bridge to a vehicle raises a number of questions. Firstly, it may be difficult to record the difference in the deflection signal between a healthy and a slightly damaged structure to the required level of accuracy and high scanning frequencies in the field. Secondly, the bridge is going to have a road profile and it will be loaded by a sprung vehicle and time-varying forces rather than a constant load. Therefore, an algorithm based on a plot of wavelet coefficients versus time to detect damage (a singularity in the plot) appears to be very sensitive to noise. This paper addresses these questions by: (a) using the acceleration signal, instead of the deflection signal, (b) employing a vehicle-bridge finite element interaction model, and (c) developing a novel wavelet-based approach using wavelet energy content at each bridge section which proves to be more sensitive to damage than a wavelet coefficient line plot at a given scale as employed by others.

Keywords: Bridge, Damage detection, Wavelet, Moving Load, Dynamics, Acceleration

Corresponding author: David Hester
Email: david.hester@ucdconnect.ie
Tel: 00353 1 716 3233
Fax: 00353 1 7163297

Nomenclature

A_c	wavelet energy content per strip interval
{a}	vector of corrupted accelerations
$\{a_{calc}\}$	vector of noise-free accelerations
a_0	mass related Rayleigh damping coefficient
a_1	stiffness related Rayleigh damping coefficient
[C]	global damping matrix
delta	ratio of crack height to overall beam depth
E_p	level of noise added to the signal
F_s	wavelet pseudo frequency corresponding to scale 's'
F_c	wavelet centre frequency
{F(t)}	vector of applied forces
[K]	global stiffness matrix
L	bridge span
[M]	consistent global mass matrix
m	Number of vanishing moments
{N}	standard normal distribution vector with zero mean value and unit standard deviation
s	wavelet scale
W	wavelet transform
x(t)	distance of the load from the left hand support at time t
x(t)/L	normalised position of the load on the bridge
Y	Transformed quantity of y
y	vector of vertical displacement and rotation of the model nodes
Δ	sampling period used to record the signal
ξ	damping ratio
σ	standard deviation of the noise-free accelerations
ω_1	1^{st} bridge natural frequency
ω_2	2^{nd} bridge natural frequency

1. INTRODUCTION

1.1 Main Aims

The objective of this paper is to investigate the possibility of using the bridge acceleration signal due to a vehicle crossing the bridge, to determine whether or not the bridge is damaged. It has been shown by Zhu and Law [1] that the wavelet transform could be employed to detect damage in a beam using the displacement response to a moving constant load. They showed that a plot of wavelet coefficients versus time at an appropriate scale allowed them to identify a singularity that was associated to the location of the damaged section. This paper builds on their work to further develop a wavelet-based damage detection algorithm in more complex scenarios such as the response of a bridge to a moving vehicle. In the latter, it is required to address a number of issues:

(a) The technique proposed by Zhu and Law uses deflections as the input signal. On a bridge site, it may not be easy to record deflections to the required level of accuracy and at high scanning frequencies. Therefore this paper investigates the use of accelerations as the input signal.

(b) The previous work was based on the response of a beam to a moving load applied as a constant force. In this paper, the moving load is modelled as a rigid sprung vehicle model with 4 degrees of freedom (DOFs) allowing for axle hop and frame bounce and pitch. A road profile is also included in the analysis. The vehicle-bridge dynamic interaction (VBI) problem is then solved using a Wilson-θ integration scheme. The results of the VBI simulations provide the input for the wavelet-based damage detection algorithm. Typical bridge and vehicle properties are employed.

(c) In Zhu and Law [1], some small cracks were detected but most of their investigation focused on large cracks, typically in the order of a crack height to beam depth ratio of 0.5. The beam used in their study had a span of 50 m and the speed of the load ranged from 0.5 m/s to 4 m/s. In this paper, it is intended to reliably detect cracks with a height to beam depth ratio smaller than 0.2 in the presence of noise. In order to achieve this level of sensitivity to damage, the authors propose a novel technique that uses wavelet coefficient versus scale plots at different points in time, rather than wavelet coefficients versus time/space plots usually found in the literature [1,2]

1.2 Detecting Damage using the Wavelet Transform

1.2.1 Background

Fig. 1 shows the mid-span acceleration response of a healthy 40 m beam (delta = 0.0) as it is traversed by a constant load of 10 tonnes moving at 3 m/s. In this paper, delta refers to the ratio of crack height to overall beam depth, so delta = 0.0 indicates that the section is uncracked, whereas delta=0.5 implies that 50% of the section is cracked. The x-axis in the figure shows the normalised position of the load (x(t)) on the bridge with respect to the bridge length (L) (0 and 1 when the load is at the start and end of the bridge respectively). The properties of the 40 m beam are those typical of a 15 m wide bridge

consisting of 10 No SY6 precast concrete beams spaced at 1.5 m centres with a 195 mm thick deck slab [3], resulting in an inertia of 6.02 m^4, a Young's modulus of $3.5x10^9$ N/m^2, and a total cross sectional area of 10 m^2. The figure also shows the acceleration signal when the same bridge has a crack at the third point of the span (delta = 0.5). This damaged has been introduced following recommendations by Sinha et al. [4], where it is assumed that damaged is extended over a region of three times the beam depth. This region has a gradual reduction in stiffness down to a minimum at the cracked section.

(Approximate location of Figure 1)

Damping is assumed to be negligible and the first natural frequencies of the healthy and damaged bridges, which responses are illustrated in Fig. 1, are 2.88 Hz and 2.5 Hz respectively. When the Fourier transform is applied to a signal, it defines the different frequencies present in the signal but it gives no time information. It does not show if a given frequency is present for the full duration of the signal or if it is present for just for a short period. Although the Short-time Fourier transform addresses this limitation, resolution problems remain. Wavelet analysis was developed to give better frequency-time information about a signal. Hou et al [5] gives some informative examples that demonstrate the capacity of the wavelet transform to capture frequency-time information. The mathematical definition of the wavelet transform and a description of the most common wavelets is illustrated in the literature [6,7,8]. A wavelet is a waveform of effectively limited duration that has an average value of zero:

$$\int_{-\infty}^{+\infty} \psi(x)dx = 0 \qquad (1)$$

where $\psi(x)$ is the mother wavelet and it is from this function that the analysing wavelets, $\psi(x)_{\bar{x},s}$, can be obtained by scaling $\psi(x)$ by s and translating $\psi(x)$ by $\bar{x}$:

$$\psi(x)_{\bar{x},s} = \frac{1}{\sqrt{s}}\psi\left(\frac{x-\bar{x}}{s}\right) \qquad (2)$$

where s is the scaling parameter and $\bar{x}$ is the translation parameter. The wavelet mother can be a real or complex function, however, in this study only real wavelets are used, and the Continuous Wavelet Transform (CWT) corresponding to a signal $y(x)$ is given by the following Equation:

$$Y(x,s)_W = \int_{-\infty}^{+\infty} y(x)\,\frac{1}{\sqrt{s}}\psi\left(\frac{x-\bar{x}}{s}\right)dx \qquad (3)$$

$Y(x,s)_W$ refers to the transformed quantity of y(x) using the wavelet $\psi(x)_{\bar{x},s}$. In practical terms, the way a wavelet transform works is as follows: The wavelet $\psi(x)_{\bar{x},s}$ is compared to a portion of the original time series signal $y(x)$, and the wavelet coefficient $Y(x,s)_W$ is calculated. $Y(x,s)_W$ represents how closely the wavelet is correlated with this portion of the signal. The entire length of the signal is checked resulting in a plot of the wavelet

coefficients versus time. Then the wavelet is scaled (i.e., stretched) and the process is repeated. Ultimately, the wavelet transform returns a wavelet coefficient for each scale at each point in time. When the wavelet transform is applied to a continuous time series signal, the result is a 3-dimensional surface. In this plot, time and scale can be represented on the two mutually perpendicular horizontal axes, and wavelet coefficient on the vertical axis. However, it is more common to represent the 3D wavelet surface as a 2D contour plot. Fig. 2 shows the result of a wavelet transform performed on the healthy signal shown in Fig. 1. In this figure, the horizontal axis gives the normalised position of the load on the bridge (x(t)/L is the distance between the load and the left hand support at any time, divided by the length of the bridge). The vertical axis shows the range of scales used in the wavelet transform. The magnitude of the absolute value of the wavelet coefficient at a given scale, *s*, for a particular location of the load in time is indicated using a lighter colour for higher values of $Y(x,s)_W$.

(Approximate location of Figure 2)

A high scale implies stretched wavelet, therefore slowly changing features, and the coefficients associated to a high scale will correspond to a low frequency content. Conversely a low scale implies a high frequency. Therefore, it is possible to relate the wavelet scale to a pseudo frequency, and a high wavelet coefficient at a particular scale will be an indication of the frequency content of the signal at this time. Equation (4) relates the scale of a wavelet to pseudo frequency. Therefore by looking at the wavelet transform and identifying the scales giving high values of wavelet coefficients, it is possible to estimate the frequencies that are present in the signal.

$$F_s = \frac{F_c}{s\Delta} \qquad (4)$$

where F_s is the pseudo-frequency corresponding to scale s in Hz, F_c is the centre frequency of the wavelet in Hz (Centre frequency effectively means the frequency of a periodic signal that most closely resembles the wavelet), s is the scale of the wavelet, and Δ is the sampling period used to record the signal. In Fig. 2, which has been generated using the Mexican Hat wavelet, it is evident that at a scale of approximately 173, there is a series of dominant peak values for the wavelet coefficients. For the Mexican Hat wavelet, $F_c = 0.25$ Hz, and $\Delta = 0.0005$ seconds, which for a scale of 173 results into a pseudo-frequency of 2.89 Hz. The latter is the 1st natural frequency of the bridge.

1.2.2 How wavelets detect damage

Damage in a structure can lead to localised singularities in the response signal of the structure. In terms of why there should be a singularity in the acceleration response, it is useful to distinguish three different components: ’static’, ‘damage’ and ‘dynamic’. Here, the ‘static’ component refers to the response that would be experienced at the measurement location if the load was moved incrementally across the ‘healthy’ structure without considering the contribution of inertial forces of the bridge (i.e., null vibration). The ‘damage’ component is the increment in the ’static’ response experienced at the measurement location due to the damaged portion of the beam. It must be noted

that the ‘damage’ component will be relatively small in relation to the ‘static’ component and the maximum value of the ‘damage’ component will occur when the load is located over the damaged location. The ‘dynamic’ component is simply the part of the total response that can be attributed to the vibration of the bridge. The ‘static’ and the ‘damage’ components of the acceleration signal are very small compared to the ‘dynamic’ component. However, in a frequency range far away from the main mode of vibration of the bridge, the ’static’ and ‘damaged’ components of acceleration become more visible compared to the ‘dynamic’ component as a wavelet analysis demonstrates. While the ‘static’ component increases continuously from zero to a maximum at the measurement location and then decreases linearly back to zero, the ‘damage’ component is zero everywhere except around the damaged portion of the bridge. These non-zero values associated to the ‘damage’ component are the cause of the singularity being sought here.

A significant advantage of the wavelet transform is its ability to capture frequency- time information and to analyze a localized portion of a larger signal. Many authors have used the wavelet transform to identify if there were singularities present in the response signal and thereby locate damage [9,10,11]. Hou et al [5] detect damage in a structure using the Discreet Wavelet Transform (DWT). The DWT splits the input signal into ‘approximations’ (low frequency components) and ‘details’ (high frequency components). The structure in question is a single degree of freedom mass-damper-spring system with multiple parallel springs. Each spring in the system has a threshold value and if the structural response exceeds this threshold value the spring will break. It is shown that if the acceleration signal of the system is analysed using a wavelet transform the instant of spring failure can be correctly identified. A number of authors were able to identify the location of damage in a beam by analysing its mode shape using the CWT [8,9,12]. Douka et al [13] analyse the mode shape data of a cantilever beam using the CWT to locate the damage and to estimate its severity. Douka et al [14] use a similar approach to detect damage in a plate with an all over part through crack, (i.e. plate is cracked across its full width). The mode shapes for the damaged plate are generated using a numerical model. These mode shapes are then analysed using a wavelet transform and the location and severity of the damage are estimated Ruka and Wilde [15] successfully detect a localised area of damage in a plate by applying a 2-dimensional wavelet transform to the fundamental mode shape of the plate.

Haung et al [16] used the 2-dimensional wavelet transform to detect multiple damaged locations in a plate. The displacement response of the damaged plate to a static load was simulated using a numerical model and knowledge of the healthy displacement response was assumed. Individual damage locations were identified by subtracting the displacement of the healthy plate from the displacement of the damaged plate, and then, analysing the displacement variation with a 2-dimensional wavelet transform. A number of authors have combined wavelet analysis with neural networks in an attempt to develop more reliable structural health monitoring techniques. Sun and Chang [17] use wavelet analysis and neural networks to detect damage in a structure. Reda Taha et al [18] use a combination of neural networks and the discreet wavelet transform to detect damage in a bridge, where the response of the bridge is modelled numerically. A similar approach was

used by Reda Taha to detect damage in the ASCE benchmark structure using phase II experimental data [19]. In [18] and [19] it is shown that using the energy of wavelet decomposed acceleration signals as a damage feature for structural health monitoring is an effective approach. Azarbayejani et al [20] also successfully use the energy of an acceleration signal as a damage feature for damage detection. The impact of measurement noise has also been investigated [5,13]and it is generally reported that the singularity due to damage is difficult to establish in scenarios with small damage and/or the interference of noise.

Much of the previous work on detecting damage in beams and plates using dynamic measurements has focused on mode shape data and where accurate mode shape data was available, the wavelet technique was able to identify and locate damage. However, noise, spectral leakage, an inability to measure at all desired locations and/or a limitation in the number of measurements due to the cost/time involved in the testing may prevent the extraction of accurate mode shape data

The question of which wavelet base to use in a damage detection analysis is addressed by [9] and [13], who point out that the answer is related to the concept of vanishing moments. A wavelet is said to have m vanishing moments when Equation (5) holds:

$$\int_{-\infty}^{+\infty} x^k \psi(x) dx = 0, \qquad k = 0,1,2,3 \dots ., m-1 \qquad (5)$$

It follows that each wavelet will have at least one vanishing moment (Equation (1)). When a wavelet is characterised by fast decay and m vanishing moments, Mallat [7] shows the existence of a function θ(x) such that

$$\psi(x) = (-1)^m \frac{d^m \theta(x)}{dx^m} \qquad (6)$$

Following on from Equation (6), Mallat also shows that Equations (7) and (8) hold.

$$\int_{-\infty}^{+\infty} \theta(x) dx = K \neq 0 \qquad (7)$$

$$\lim_{s \to 0} \frac{Y(x,s)_W}{s^{m+\frac{z}{2}}} = K \frac{d^m y(x)}{dx^m} \qquad (8)$$

A table showing the properties of a number of different wavelet bases is given in [15]. Gentile and Messina [8] and Pakrashi et al [9] investigate how the performance of different wavelet families relates to the numbers of vanishing moments in damage detection problems. [8] highlight the significance of Equation (8) by pointing out that when scale, s, has been fixed to a comparably small value, $Y(x,s)_W$ is likely to be a good

approximation of $Ks^{m+1/2}$ times the m^{th} derivative of the signal y(x) Therefore, for the lowest values of scale, *s*, a wavelet with only one vanishing moment will distinguish features in y(x) that are related to the first derivative of the signal. More vanishing moments are required to capture higher order derivatives. [8] and [9] found that when the Haar wavelet (only one vanishing moment) was used in the analysis, a local jump in the wavelet coefficients was observed at the location of the damage, rather than the local extremum observed for wavelets with a greater number of vanishing moments. In most cases the order of the derivatives to be detected do not exceed 2, so typically wavelets with 2 vanishing moments will suffice [13] In the review by Reda Taha et al [11], it is observed that there is no unique wavelet that can satisfy all structural health monitoring requirements and that some wavelets perform better in certain situations than others. Therefore, the choice of wavelet is generally governed by a desire to maximise the damage feature being used to detect damage. With this in mind the dynamic response of a damaged beam was analysed using a number of different wavelet bases (Daubechies 2 (m=2), Symlets 2 (m=2), Coiflets 2 (m=2), Gaussian 2 (m=2), and Mexican Hat (m=2). It was found that Gaussian 2 and Mexican Hat were the most successful at identifying the type of damage investigated in this paper. Although the Gaussian 2 and Mexican Hat wavelet had a similar level of performance, ultimately it was decided to use the Mexican Hat wavelet throughout the paper, given its proven ability to identify damage in similar problems [1,21,22].

Fig. 3 shows a contour plot of the wavelet coefficients obtained when the continuous wavelet transform is applied to the damaged acceleration signal shown in Fig. 1. There is a local increase in the absolute value of the wavelet coefficients as the load passes over the crack. However, this increase is only evident at scales appreciably greater than the scale corresponding to the first natural frequency.

(Approximate location of Figure 3)

A coefficient line plot shows how the wavelet coefficients vary with time at a particular scale. Fig. 4 shows the coefficient line plot at a scale of 700 (pseudo-frequency of 0.71 Hz) for both the healthy and damaged signals. When there is no damage in the beam (delta = 0.0), a practically horizontal line is obtained. However, in the damaged case (delta = 0.5), there is a clear peak in the wavelet coefficients at 0.33 which is the location of the damage.

(Approximate location of Figure 4)

It is important to note the figures shown so far are somewhat simplified in the sense that the signals were produced using a simple moving constant load model, the cracks modelled were large and no noise was added to the signal. However, they are used here to demonstrate the fundamental principles behind the detection of damage using wavelets. In the following sections, the technique will be tested in more realistic

situations that increase the difficulty of detecting damage, i.e. noisy signals, smaller damage and simulated signals from VBI models.

2. TESTING WITH SIMULATED BEAM ACCELERATIONS DUE TO THE CROSSING OF A CONSTANT LOAD

2.1 Mathematical Model of the Vehicle-Bridge System

The dynamic response of a bridge subject to a moving load is solved using the second order matrix differential equation given in Equation (9).

$$[M]\left\{\frac{d^2y(t)}{dt^2}\right\} + [C]\left\{\frac{dy(t)}{dt}\right\} + [K]\{y(t)\} = \{F(t)\} \qquad (9)$$

where y contains the vertical displacement and rotation of the model nodes, [M] is the consistent global mass matrix, [C] is the global damping matrix, [K] is the global stiffness matrix and {F(t)} is the vector of applied forces. The first step is to populate the global stiffness and mass matrices of the bridge. The elementary stiffness and mass matrices for 1D beam elements are well established [23]. It is considered that the global mass matrix of the structure is unaffected by the presence of a crack. However, the presence of a crack will result in a localised loss in bending stiffness in the vicinity of the crack and the global stiffness matrix for the structure needs to reflect this. Crack modelling approaches try to represent the loss in stiffness due to the crack [24,25]. If using beam elements to model the structure, there are 3 common approaches to modelling the crack that are examined in [9]. Spring crack models represent the crack using a rotational spring [26,27]. Smeared crack models represent the loss in stiffness by uniformly reducing the moment of inertia over a given length [28]. Continuous crack models try to allow for the continuous reduction in stiffness as the crack is approached [4,29] and this is the modelling approach adopted in this paper. The specific continuous crack technique used was that proposed by Sinha et al. [4], which it is based on the work of Christides and Barr [30]. For a notched rectangular beam, Christides and Barr described the fall of in bending stiffness as one approached the notch as having an exponential profile, approximated with a straight line by Sinha. Sinha assumes the distance either side of the crack that experiences a loss in stiffness to be 1.5 times the depth of the beam. Then, using these values of bending stiffness in the vicinity of the crack, the elemental stiffness matrices of the damaged elements were calculated and the global stiffness matrix for the structure was populated. Sinha's approach was developed for rectangular beams, where a given ratio of crack height to beam depth implies a certain loss of stiffness, e.g., when the crack height is 10% of the total section depth the inertia at the damaged location can be shown to be 71% of the inertia at a healthy location. In this paper, other types of sections are employed, although the traditional notion of crack height to beam depth is maintained as a measure of damage severity to be consistent with previous published work allowing meaningful comparison of results.

(Approximate location of Figure 5)

A constant load P crosses the structure at a given speed and {F(t)} defines the distribution of P to the DOFs nearby at each time 't'. {F(t)} is calculated by determining the position of the load (b(t)) at every time step and using the hermitian shape functions to apportion the applied load to the nodes of the beam element where the load is located. Fig. 5 shows the arrangement of the model. In order to perform a dynamic simulation of a load crossing the bridge it is necessary to convert the equilibrium equations of motion into a discrete time integration scheme. This scheme is solved using the Wilson-θ method which is described in [31]. The results of the beam response to the moving load were found to be in agreement with those published by Mahmoud [26] for different crack depths of a 50 m simply supported beam. Measurements from a field test will contain noise, which is added here to the simulated acceleration using the additive model proposed by [1], as given by Equation (10).

$$\{a\} = \{a_{calc}\} + E_p\{N\}\sigma \quad (10)$$

where {a} is a vector of corrupted accelerations, $\{a_{calc}\}$ is a vector of noise-free accelerations, E_p is the noise level (3% is adopted in this paper), {N} is a standard normal distribution vector with zero mean value and unit standard deviation, and σ is the standard deviation of the noise-free accelerations. Acceleration signals were simulated at mid-span for a scanning frequency of 2000 Hz, which is within the operative range of modern accelerometers. The damage levels being modelled here could be detected using lower scanning frequencies, however, the impact of Gaussian noise on damage identification may result significant if the number of available measurements is reduced.

2.2 The use of the Coefficient Line Plot as Damage Detection Tool

The signals in Section 1 were chosen primarily for illustration purposes as there was no noise and the cracks modelled were large. They showed that the wavelet transform could only detect damage at scales that were significantly higher than the scale corresponding to the 1st natural frequency of the bridge. At scales near or below the first natural frequency of the bridge, there will typically be much interference derived from the vibrations of the main mode of vibration of the bridge and noise that will prevent the identification of a singularity. Fig. 6 shows the healthy and damaged mid-span acceleration signal of the 40 m bridge described in Section 1.2, that is subject to a 10 tonne constant load moving at 3 m/s with 3% noise added to both signals. In the damaged case, the bridge has a crack at the 1/3 point of the span with delta = 0.3. The 1st natural frequency of the healthy bridge is 2.88 Hz. The 1st natural frequency of the bridge is 2.68 Hz when there is a delta = 0.3 crack at the 1/3 point (i.e., a 6.9% decrease with respect to healthy structure). Damages of delta = 0.1 and 0.2 at the 1/3 point of the span result in 1st natural frequencies of 2.82 Hz (2.1% decrease) and 2.76 Hz (4.2% decrease) respectively.

(Approximate location of Figure 6)

The singularity in the damaged acceleration signal is not visible to the naked eye, but when a wavelet transform is carried out on the signal there is a series of high wavelet coefficients evident at the 1/3 point (Fig. 7(a)). Fig. 7(b) shows the coefficient line plot when delta = 0.1 at the 1/3 point. Both coefficient line plots correspond to a scale of 700. It can be seen that the presence of noise results in a far less smooth coefficient line than when the acceleration signal contained no noise (Fig. 4). Therefore, when the damage is small (Fig. 7(b)), the singularity due to the damage may appear masked by noise, and the coefficient line approach will result insufficient.

(Approximate location of Figure 7)

2.3 The use of Vertical Sections of the 3-D Wavelet Surface to Detect Damage

It has been shown a coefficient line plot (a horizontal section of the 3-D wavelet surface) may result inefficient for detecting small damages in the presence of noise. However, it can be seen in Fig. 3 that the singularity exerts its influence not only at one scale but across a broad range of scales from approximately 500 to 1200 (pseudo-frequencies of 1 Hz and 0.416 Hz respectively). This is demonstrated in Fig. 8 by taking a series of vertical sections through the 3-D wavelet surface. This increase in wavelet coefficient across a range of scales is exploited to improve the sensitivity of the algorithm to small damages. Fig. 8(a) shows the wavelet transform surface obtained when the bridge has a delta = 0.2 crack at the 1/3 point of the span. Fig. 8(b) shows five different vertical sections through the wavelet transform surface from scales 1-1200. At each section a peak occurs at a scale of approximately 173 (scale corresponding to the 1st natural frequency) and low value of wavelet coefficients are obtained at scales greater than 500. Fig. 8(c) shows a magnified view of the wavelet coefficients for the range of scales between 500-1200.

(Approximate location of Figure 8)

From the point of view of damage detection it is the scales 500 to 1200 that prove to be most useful. It can be seen that the wavelet coefficients at $x(t)/L = 0.3$ (which is the closest to the damaged section at 0.33 of all vertical sections under investigation) are significantly higher across this range of scales than at any of the other locations. If the area under each of the curves shown in Fig. 8(c) was calculated, the area under the 0.3 curve would be significantly larger than the area under any of the other curves. However, calculating the area under individual sections taken at regular intervals could be very sensitive to noise for low levels of damage, so a more systematic approach is necessary. So, the 3D wavelet surface is broken up into a series of strips at different points in time. Each of these strips corresponds to a particular location of the load on the bridge. For example, a strip A of the wavelet transform surface is assumed to correspond to a load location between 0.2L and 0.3L, strip B corresponds to a load location between 0.3L and 0.4L and so on (Fig. 9). The average area under each strip is determined by first calculating the average wavelet coefficient of the strip at each of the scales used in the wavelet analysis (these average values are marked for a strip C as grey dots in Fig. 9 and

they have the benefit of reducing the influence of noise across the strip) and then, finding the area under curve C defined by the average wavelet coefficients (A_c). The sensitivity of the algorithm can be further improved using the square of the wavelet coefficient (also known as wavelet energy spectrum [32]) for each of the grey dots to compute the area A_c.

(Approximate location of Figure 9)

There will be one value of wavelet energy content per strip interval, (i.e., the area under the wavelet spectral energy curve). If there was damage in a particular interval of travel on the bridge, the wavelet energy content for the damaged strip interval should be the largest. If Figures 2 and 3 are examined, there appears a series of high wavelet coefficients across all scales at the edges of the signal. These edge effects prevent the coverage of those portions of the bridge close to the supports. However, in a simply supported span if flexural cracking is to occur, it is most likely to develop in the middle third of the span where stresses are higher, therefore only the portion of the 40 m bridge between 0.2L to 0.8L is analysed. In the figures that follow the load is applied as a constant 10 tonne load travelling at 3 m/s with 3% noise added to the acceleration signal. The bridge has a crack with delta = 0.1 at 1/3 point. Fig. 10 shows the total wavelet energy content between scales of 500 and 1500 associated to consecutive strips, 0.5 m long each. In this figure, there is a peak as the load passes over the damage at the 1/3 point of the span and there is also a peak, slightly shifted to the right, related to the passage of the load over the sensor positioned at mid-span. The individual wavelet energy values are sensitive to noise (larger values for larger levels of noise), so it is recommended to subtract the mean energy from the individual energies computed in Fig. 10. The resulting relative energy plot is shown in Fig. 11. This figure also shows the results obtained when the mid-span acceleration signal from a healthy bridge is analysed which exhibits only the peak at the sensor location. Using this wavelet energy content per strip procedure, the damaged response reveals a distinctive peak that the coefficient line plot was unable to appreciate (Fig. 7(b)).

(Approximate location of Figure 10)

(Approximate location of Figure 11)

The fact that the load passing over the sensor results in a peak at the sensor location can be misleading, i.e., a peak does not necessarily indicate damage if it is associated to the observation point. This limitation can be overcome by using multiple sensor locations. Therefore, results can be drastically improved if the acceleration signal was collected at three locations simultaneously. A wavelet transform is carried out on each signal resulting in a relative energy plot for each signal, and then the three relative energy plots can be averaged to give the final result. Fig. 12 illustrates the resulting curves from three sections located at the ¼, mid-span and ¾ point of the bridge length. The loading arrangement and structural conditions are the same as those used to generate Fig. 10. There is a number of observations to be made about Fig. 12, firstly, it can be seen that

regardless the observation point, the singularity due to the damage is picked up to some extent. It can be seen that the peak at 0.33L is quite small for the signal simulated at the ¾ point due to the relatively far distance from the damaged section. The closer the sensor is to the damage the better it is identified (i.e., ¼ span compared to ¾ span). The effect of averaging the plots of all sensor locations is to minimise those undesired peaks due to the load passing over the sensors and magnifying the peak at the damaged location (bold line in Fig. 12). Fig. 13 shows the result obtained when averaging the results from the quarter point, mid-span and three quarter point acceleration signals for different levels of damage. While the healthy bridge has no evident peaks, a bridge with a delta = 0.1 crack at the third point has a small but noticeable peak at the damaged location, and a bridge with a delta = 0.2 crack has a very distinctive peak.

(Approximate location of Figure 12)

(Approximate location of Figure 13)

To investigate the impact of scanning frequency, acceleration signals were simulated for scanning frequencies of 500 Hz and 1000 Hz. It was found that in the absence of noise a scanning frequency of 500 Hz was as successful as 2000 Hz in identifying a clear peak for a damage of delta = 0.1. When the acceleration signals contained 3% noise, scanning frequencies of 500 Hz and 1000 Hz were also able to detect a delta = 0.2 crack. For a scanning frequency of 1000 Hz and 3% noise, it was possible to identify damage of delta = 0.1. In the latter, the peak was less distinct with respect to other peaks in the processed signal when compared to a scanning frequency of 2000 Hz. When a scanning frequency of 500 Hz and 3% noise was used, the peak associated to a damage of delta = 0.1 was difficult to distinguish from other peaks related to noise. Essentially, it was found that the impact of Gaussian noise becomes more significant when trying to detect the lowest levels of damage with a lower scanning frequency.

The range of scales used to detect damage in Fig. 13 was 500-1500. The lower scale limit was chosen so as to avoid interference from the main bridge frequency (see Fig. 8) i.e., at this scale the area of influence of the first natural frequency of the bridge has disappeared. Essentially, the lower scale limit used was 2.89 times the scale corresponding to the 1st natural frequency (2.89 x173 = 500). However, at very high scales, there is a loss of resolution and as a result, loss of accuracy in the location of the singularity associated to damage. The upper scale limit for damage detection was 1500, i.e. 8.67 times the scale corresponding to the first natural frequency (8.67 x 173 = 1500). These scale ratios were then applied to 10 m and 20 m bridge theoretical models to check if they could be used as reference when detecting damage in other spans.

10 m and 20 m bridge models were found to have 1st natural frequencies of 10.4 Hz and 6.4 Hz respectively. Acceleration signals were simulated in the same manner as for the 40 m bridge, i.e., as a result of a 10 tonne point load moving across the bridge at 3 m/s. Acceleration signals were simulated at the ¼ point, mid-span and ¾ point, the scanning frequency used was 2000 Hz and 3% noise was added to all acceleration signals. Following wavelet transform of the acceleration signal, the scale corresponding to the 1st natural frequency of the 10 m bridge was found to be 49. If the scale ratios used to detect damage in the 40 m bridge are applied to the 10 m span, lower and upper scale limits of 140 (2.89 x 49) and 425 (8.67 x 49) respectively are obtained. The results of

using these scale limits are shown in Fig. 14 and it can be seen that the range of scales 140 – 425 are effective at detecting damage in the 10 m bridge. After carrying out the wavelet transform on the acceleration signals from the 20 m bridge the scale corresponding to the 1st natural frequency was found to be 79. Lower and upper scale limits of 230 and 680 result from applying the scale ratios developed for the 40 m bridge. Fig. 15 shows how the damage is again accurately located using those scale ratios. Although the scale ratios employed here were found to be effective for the bridges being modelled, it is not suggested that they define the optimum range of scales for every bridge and they are only provided as guidance on a reasonable range of values to be selected. Figs. 13, 14 and 15 also demonstrate that the proposed damage detection technique can be successful across a range of bridge spans.

(Approximate location of Figure 14)

(Approximate location of Figure 15)

2.4 Influence of Damping and Multiple Damage Locations

The case of damage detection in the presence of undamped bridge accelerations (i.e., [C] = [0] in Equation (9)) has been investigated in previous sections. Here it is shown that the damage detection algorithm has a similar performance when applied to damped vibrations. Equation (9) gives the second order matrix differential equation that governs the dynamic response of a bridge subject to a moving load. Rayleigh damping is adopted to calculate the damping matrix as a combination of the global mass and stiffness matrices, as shown in Equation (11).

$$[C] = a_0[M] + a_1[K] \qquad (11)$$

where $a_0=2\xi\omega_1\omega_2 / (\omega_1+\omega_2)$, $a_1=2\xi / (\omega_1+\omega_2)$, ξ is the damping ratio to be simulated, and ω_1 and ω_2 are the 1st and 2nd bridge frequencies respectively [33]. It is assumed that only the first two modes of vibration are significant and the damping ratio (ξ) is the same for both modes. A typical ξ value of 0.02 for bridge structures is tested here. Fig. 16 shows the mid-span acceleration signal with damping (ξ = 0.02) and without damping (ξ = 0.00). When the load first enters the bridge, the amplitudes of vibration in the damped and undamped systems are similar, however subsequently the amplitudes of vibration in the damped system fall off rapidly. The damping matrix was calculated using the healthy global stiffness matrix and the same damping matrix was used for all damage levels.

(Approximate location of Figure 16)

Fig. 17 shows the result of applying the damage detection technique described in Section 2.3 to damped acceleration signals (ξ = 0.02). Fig. 17 is analogue to Fig. 13, although the peaks due to the damped acceleration signals are slightly more pronounced than the ones

observed in Fig. 13 for the range of scales used in the analysis. The peak heights for delta = 0.1 and 0.2 are $2.58x10^{-5}$ and $16.78x10^{-5}$ respectively in Fig. 13, while these peak heights for delta = 0.1 and 0.2 are $3.4x10^{-5}$ and $18.75x10^{-5}$ respectively in Fig. 17. Hence, the inclusion of damping appears to favour damage identification. The impact of increased damping and noise is further investigated by increasing the damping ratio (ξ) to 0.04 and increasing the level of noise to 10% ($E_p = 0.1$ in Equation (10)). The results of this analysis are presented in Fig. 18 for different levels of damage. If the plots in this figure are compared to those in Fig. 17, it can be seen that the height of the damage peaks and the shape of the plots for the different damage levels are quite similar. Hence, the technique does not appear to be particularly sensitive to changes in damping and is relatively robust with respect to noise. Damping reduces the dynamic vibrations and this reduction somehow makes it easier to detect the damage singularity in a damped signal. Nevertheless, damage can affect damping in many complex ways which are outside the scope of this paper. Therefore, having established that the consideration of viscous damping does not negatively affect the ability of the technique to detect damage, it was decided to run the simulations remaining in the paper with null damping conditions.

(Approximate location of Figure 17)

(Approximate location of Figure 18)

To investigate the performance of the technique at detecting multiple damage scenarios the bridge is modelled to allow for different damage combinations. Combination 1 has a delta = 0.1 crack at the 1/3 point of the span and a delta = 0.2 crack at the 2/3 point of the span. Combination 2 has a delta = 0.2 crack at the 1/3 point of the span and a delta = 0.1 crack at the 2/3 point of the span. Combination 3 has a delta = 0.15 crack at the 1/3 point of the span and a delta = 0.15 crack at the 2/3 point of the span. The acceleration signals from the quarter point, mid-span and three quarter point were analysed to give the plots shown in Fig. 19. In all cases both damage locations are clearly identified and the height of the peaks can be related to the severity of the damage.

(Approximate location of Figure 19)

3. TESTING WITH SIMULATED BEAM ACCELERATIONS DUE TO THE CROSSING OF A SPRUNG VEHICLE MODEL

3.1 Vehicle-Bridge Interaction Model

An iterative approach was employed to implement the VBI model [34,35]. The vehicle was modelled as a planar 2-axle rigid truck with 4 DOFs: the pitch and vertical displacement of the sprung mass and the displacement of the two unsprung masses. The contact forces between the axles of the vehicle and the road profile are obtained using the equations of motion of the vehicle [36]. Then, these contact forces are applied to the finite element (FE) model of the bridge. The structural model of the bridge is the same as

that described in Section 2.1, only that this time there are two axle loads. Once the force vector {F(t)} has been generated, the Wilson-θ method is used to calculate the displacement of each of the bridge DOFs at each time step. In a preliminary step, the contact forces applied to the FE model of the bridge are calculated using a 'stationary' road profile, i.e., no allowance is made for the fact that the axle displacement will change due to the deflection of the bridge. Using the hermitian shape functions, it is possible to calculate the vertical bridge displacement under each axle at each time step. Therefore, a new profile defined by the road irregularities in addition to the displacements of the bridge is calculated. Then by repeating the procedure using the latest bridge road profile, a new set of contact forces can be obtained. These calculations are repeated until convergence is achieved. The suspension and tyre properties of the truck are similar to those of a semi-tractor unit with twin wheels in the rear axle. Table 1 gives a summary of the different vehicle properties used in the simulations [37,38]. The road profile is an array of numbers that defines the height of the road irregularities at each time step. Cebon [39] describes how an artificial road surface topography of a given ISO roughness/classification can be generated for use in time-domain vehicle vibration simulations. In this paper, only ISO class 'A' ("very good") profiles, typical of well-maintained highways, are used.

(Approximate location of Table 1)

3.2 Wavelet Transform of Signal from Interaction Model with Smooth Road Profile

3.2.1 Original input signal

As a sprung vehicle passes over a bridge, the axle forces applied to the bridge vary, and the dynamic response of the structure will be less smooth than the case of a moving constant load. This situation will make the detection of a local singularity a more difficult task. Fig. 20 shows the mid-span acceleration signal of the bridge when it is traversed by a 15 tonne truck moving at 3 m/s on a smooth road profile (Note this signal contains 3% noise added as described by Equation (10)). The bridge is modelled as having a delta = 0.3 crack at the 1/3 point of the span. It can be seen in Fig. 20 that there is an abrupt change in the amplitude of the acceleration signal at the end of the signal as the front axle leaves the bridge (time = 13.3 s). There is a smaller change in amplitude at the start of the acceleration signal as the rear axle of the truck enters the bridge (time = 1.26 s).

(Approximate location of Figure 20)

Fig. 21(a) shows a contour plot of the wavelet coefficients obtained when the signal shown in Fig. 20 is analysed between scales of 1 and 1500 using the Mexican hat wavelet. This plot has similarities with the wavelet transform of the constant load signal shown in Fig. 3. The first natural frequency of the bridge is evident at low scales and there is a series of high wavelet coefficients at 1.26 seconds and at 13.3 seconds. The latter are not due to damage but as a result of the wavelet transform identifying the singularities in the acceleration signal due to the rear and front axles entering and leaving the bridge respectively. When modelling multi-axle vehicles, singularities at the instants at which

axles enter or leave the bridge are inevitable. Fig. 21(b) zooms into the scales between 500 and 1500. It can be seen that at scales between 500 and 1200 there are two peaks in the wavelet coefficients at 4.5 seconds and 5.8 seconds, which are the result of the passing over the damaged section of the front and rear axles respectively. Then, at scales greater than 1200 it becomes more difficult to distinguish between both peaks. Initially, when dealing with signals from the half-car model and no road profile, the range of scales between 500 and 1100 offered good resolution in detecting damage. However, the range of scales 500-1200 became very noisy in the presence of a rough surface due to the interference of road frequencies. The existence of a rough surface requires the use of higher scales to detect damage. One disadvantage of operating at higher scales is their lower resolution when determining the exact location of the damage.

(Approximate location of Figure 21)

3.2.2 Padding of the original input signal

The large singularities in the acceleration signal due to the axles entering and leaving the bridge generate very high wavelet coefficients locally which tend to mask any damage that might be present close to the supports. In an attempt to reduce the influence of these local areas, the simulated acceleration signal can be modified using a padding technique before carrying out the wavelet transform. The first step of the technique is to remove the parts of the signal that contain the axle singularities. So, only the signal portion between 1.26 seconds and 13.3 seconds of Fig. 20 is considered, and the wavelet transform associated to the shortened signal is shown in Fig. 22. Although the axle singularities have been removed, there are still significant edge effects. These edge effects typically occur when a finite length time series is analysed with wavelets [40]. Consequently, the 'window' for detecting damage becomes quite narrow, i.e., damage could only be detected in a limited zone around the centre of the bridge. Therefore, the second step of the technique is padding the signal to reduce the influence of edge effects and to increase the length of the bridge being covered.

(Approximate location of Figure 22)

Meyers et al. [41] suggest using a form of padding that matches the endpoint frequency, amplitude and phase. Therefore the shortened signal with starting point the entrance of the 2nd axle on the bridge and ending point the leaving of the 1st axle off the bridge can be padded by identifying for example the first four cycles of vibration. Then, the start and end of the signal are extended with a repetition series of the first and last four cycles respectively as shown by Fig. 20. The centre portion of the signal in Fig. 20 (solid line) is broadly the same as that shown in Fig. 20, except that in Fig. 20 a moving average filter has been applied to this part of the signal. Provided the span of the filter was small enough, the moving average filter will remove some of the noise from the signal without removing the singularity, thereby making it easier to locate the damage using the wavelet transform. In this analysis the time step used was 0.0005 seconds and the moving average filter had a span of 27 (27*0.0005 = 0.0135 s resulting into a

frequency of 1/0.0135 = 74 Hz). Fig. 24 shows the wavelet transform of the padded signal shown in Fig. 23, where only the area between a time of 1.26 seconds and 13.3 seconds is relevant. When compared to Fig. 22 (where the true shortened signal is analysed directly), it can be seen that the edge effects at 1.26 seconds and 13.3 seconds have been noticeably reduced by padding. In practical terms, padding the signal has the effect of moving the edge effects away from the zone of interest.

(Approximate location of Figure 23)

(Approximate location of Figure 24)

3.2.3 Performance of the algorithm

To detect damage in a bridge loaded with a half-car model the same process used when analysing signals from a constant load model is employed. Again the acceleration signal is generated at three locations simultaneously (quarter point, mid-span and three quarter point) as the truck passes over the bridge, and each of the three signals are shortened and padded before being analysed using the wavelet transform. Then, the results from the three measuring locations are averaged. Scales between 1200 and1500 are employed in this analysis. Fig. 25 shows the results obtained for different levels of damage at different locations. The x-axis in the figure shows the normalised position of the mass centre of gravity of the vehicle on the bridge.

(Approximate location of Figure 25)

Fig. 25 shows that when using scales of 1200-1500 the technique can successfully detect damage and as expected, the magnitude of the relative wavelet energy for a given strip increases with more severe damage. However, it is noticeable that when analysing acceleration signals from the halfcar model at high scales, it is more difficult to precisely locate the damaged section than when using signals from a single P-load model, which could be analysed at lower wavelet scales. For example if the plot for delta = 0.2 in Fig. 13 was examined, there is a narrow peak just at the location of the damaged section. In Fig. 25, the delta = 0.2 crack is located at 0.5L, but instead of getting a narrow peak at just 0.5L a broad peak extending from approx 0.45L to 0.55L results. If Fig. 21(b) is examined, the reason for getting a broad peak in Fig. 25 can be understood. Essentially, as each axle passes over the damage there is a small singularity in the acceleration signal. At scales of between 500 and 1000 the wavelets are short enough that they can detect each singularity individually so there is a peak in the wavelet coefficients per axle. However, at scales greater than 1200 and low levels of damage (i.e., delta 0.1 at 0.33L in Fig. 25), the length of the wavelet being used in the analysis is too long to be able to separate two small singularities that are so close together, and consequently, they are in effect interpreted as one broad singularity. For damages of delta = 0.2 and delta = 0.3, the influence of the individual axles is not completely lost and the top of the peaks have twin crests.

3.3 Wavelet Transform of Signal from Interaction Model with Road Profile

Here the road profile has an ISO class 'A' (Fig. 26(a) shows the portion of the road profile on the bridge) and a crack of delta = 0.3 is modelled at the 1/3 point of the span. Fig. 26(b) shows the mid-span acceleration signal of the bridge when it is traversed by a 15 tonne truck moving at 3 m/s (3% noise has been added to this signal). If the acceleration signal shown in Fig. 26(b) was compared with the one shown in Fig. 20, it is noticeable that the road irregularities can lead to interferences in the acceleration signal which have a greater effect than a singularity due to damage.

(Approximate location of Figure 26)

Fig. 27 shows a contour plot of the wavelet coefficients obtained when the signal shown in Fig. 26(b) is analysed using the Mexican hat wavelet between scales of 1 and 1500. This wavelet transform surface presents similarities with the one shown in Fig. 21(a) for a half-car travelling over a smooth profile. The influence of the 1st natural frequency of the bridge is evident at lower scales and the singularities due to the axles entering/leaving the bridge are also present at the edges of the surface. However, the difference between the two figures lies in the zone of scales between 500 and 1100. Here, this zone has become full of high wavelet coefficients due to the interference of the road profile, thereby hindering any damage singularity that could be detected at these scales before. For this reason, the use of scales greater than 1100 becomes necessary.

(Approximate location of Figure 27)

The acceleration signal is simulated at the same three locations used in Section 3.2.3. Again, each of the three signals is shortened (to remove the axle singularities), smoothed (to remove some noise) and padded (to reduce the impact of the edge effects). Fig. 28 shows the results obtained for different levels of damage at different locations. Again the x-axis in the figure shows the normalised position of the mass centre of gravity of the vehicle. Similarly to Fig. 25, the height of the peaks in Fig. 28 increases as damage gets larger, although the peaks are slightly higher in the presence of a road profile. The inclusion of a road profile brings a larger difference in the magnitude of the peaks associated to each axle. For example, the damage of delta = 0.2 at mid-span of Fig. 25, the height of the peak is approximately $4x10^{-5}$ and there is only a small undulation at the top of the peak due to a merging of the effects of both axles. In Fig. 28 for the same mid-span damage, there is a broad peak between approximately 0.45L and 0.55L. However, at the top of this peak there are individual crests of $6x10^{-5}$ when the front axle crosses the damage and $2x10^{-5}$ when the rear axle crosses the damage. This difference in the height of the axle crests is more pronounced for delta = 0.3 at the ¾ point, leading to values of $4x10^{-5}$ and $12x10^{-5}$ for the passage of each axle on the road class 'A'. When there was a

smooth road profile and delta = 0.3 at the ¾ point (Fig. 25), the height of the crests at the top of the peak were $5x10^{-5}$ and $7x10^{-5}$. A rough road profile increases the magnitude and variability of axle forces and also the variability in the height of the axle crests associated to a damaged location. To further investigate the impact of road profile the bridge is modelled as having a class 'B' road profile. Fig. 29 shows the average relative energy for various damage levels at different locations when simulating the effects of a 'B' road class. Comparing Fig. 29 to Fig. 28, it can be seen that the plot for delta = 0.0 is far rougher so that in itself makes damage identification more difficult. The plot for delta = 0.1 at 0.33L of Fig. 29 is not sufficiently different to the delta = 0.0 plot to be able to identify damage. When increasing the damage to delta = 0.2, two twin axle crests (similarly to Figures 22 and 25) can be distinguished around the damaged location. The delta = 0.3 crack at 0.66L produces a plot with a broad peak between 0.6L and 0.75L in Fig. 29. However, rather than getting twin crests at the top of the peak, it is more a case that there is a point of inflection at 0.63L and a crest at 0.7L due to the front and rear axles respectively crossing the damage.

(Approximate location of Figure 28)

(Approximate location of Figure 29)

Figures 22, 25 and 26 show that the performance of the algorithm falls off as the roughness of the road surface increases, particularly for low levels of damage. The road profile increases the amplitude and the randomness of the induced vibrations, and it can hinder the effect of the singularity due to damage.

3.4 Influence of Vehicle Speed

The speed of the vehicle is a very important parameter that influences the amplitude of bridge vibration and the length of the available acceleration signal. When increasing the speed of the vehicle, the impact of edge effects in the wavelet transform should be considered. As the speed of the vehicle is increased the acceleration signal is shortened in the time domain. In practical terms this means a narrowing of the 'window' of the wavelet transform surface that can be used for damage detection. To counteract this narrowing of the window it is very important to pad the signal to minimise the impact of edge effects. Fig. 30 shows the results obtained when the speed of the vehicle was 7 m/s. A random class 'A' road profile was used to generate the accelerations signals processed in this figure. The analysis technique was the same as that used to produce Fig. 28, where the speed of the truck was 3 m/s. In Fig. 30, it can be seen that damages of delta = 0.2 and 0.3 could be detected, however, it was not possible to detect a damage of delta = 0.1. The length of the acceleration signal is significantly shorter at 7 m/s than at 3 m/s, leading to a shorter singularity that is more difficult to detect. Lower wavelet scales able to catch higher frequencies would have been more effective at detecting short singularities. Nevertheless, the presence of high frequency components due to the rough road profile prevents the use of low scales. When the size of the singularity due to damage becomes

sufficiently large compared to those singularities induced by the road profile (i.e., delta = 0.2 and 0.3), then it becomes possible to detect those weakened sections at 7 m/s. When vehicle speeds greater than 7 m/s were tested, the algorithm lost effectiveness due to the singularity becoming shorter, vibrations often getting larger and preventing to distinguish the singularity, and the increasing impact of edge effects that padding can only partially mitigate.

(Approximate location of Figure 30)

4.0 DISCUSSION

This paper has shown that it is possible to detect damage in a 40 m simply supported bridge beam model by analysing its acceleration response to a moving load. Initially, signals from a moving constant load model were examined and it was found that the coefficient line plot (which uses only one wavelet scale) was effective at detecting large cracks, however, it was unreliable when trying to detect small levels of damage. To overcome this limitation a technique which utilised a range of scales was developed and it was found to be more sensitive to damage than using just a single scale. This technique used the acceleration signal obtained at one bridge location to calculate the average wavelet energy content for equally spaced strips across the bridge. This wavelet representation revealed that those damaged strips had a higher wavelet energy content than the undamaged strips when the appropriate range of scales was considered (i.e., away from the natural frequency of the bridge). The use of multiple sensor locations gave significantly better results than using just one sensor location.

Using the bridge acceleration due to a half-car VBI model as input signal posed two significant challenges not present in the acceleration signal from a model based on constant loads: (1) there were sharp singularities in the acceleration signal due to the vehicle axles passing on and off the bridge; (2) the presence of a road profile led to a significantly rougher acceleration signal than that generated by a moving constant load model. The problem of having singularities at the start and at the end of the acceleration signal was addressed by trimming the simulated acceleration signal to remove these singularities, and padding the remainder of the signal to reduce the impact of edge effects. The problem of a rougher acceleration signal (due to the road profile) required a reduction in the range of scales at which it is possible to detect damage. As the speed of the vehicle was increased, the algorithm lost sensitivity to a damaged-related singularity. Essentially higher wavelet scales need to be used and consequently some accuracy is lost when determining the damaged location. Even although the exact location could not be provided for some cases, it was still possible to predict a relatively narrow portion of the bridge where damage could be contained. Therefore, when the acceleration signal due to a 2-axle vehicle was simulated at the quarter point, mid-span and three quarter point of a beam model in the presence of a class ‘A’ road profile and 3% noise, a crack as small as 10% of the total section depth could still be reliably detected at 3 m/s using the proposed technique based on wavelet energy content.

Acknowledgements
The authors wish to express their gratitude for the support received from the 7th European Framework Project ASSET towards this investigation.

References

[1] X.Q. Zhu, S.S. Law, Wavelet-based crack identification of bridge beam from operational deflection time history, International Journal of Solids and Structures, 43 (2006) 2299-2317.
[2] A.V. Ovanesova, L.E. Suárez, Applications of wavelet transforms to damage detection in frame structures, Engineering Structures, 26 (2004) 39-49.
[3] Tarmac , 2009. http://www.tarmacbuildingproducts.co.uk/products_and_services/precast_concrete/bridge_beams.aspx Accessed, 4th October, 2010.
[4] K.J. Sinha, M.I. Friswell, S. Edwards, Simplified models for the location of cracks in beam structures using measured vibration data, Journal of Sound and Vibration, 251(1) (2002) 13-38.
[5] Z. Hou, M. Noori, R. St. Amand, Wavelet-based approach for structural damage detection, Journal of Engineering Mechanics, 126 (2000).
[6] I. Daubechies, Ten lectures on wavelets, CBMS Conference Series 61, SIAM, Philadelphia, 1992.
[7] S.G. Mallet, A wavelet tour of signal processing, second ed. Academic Press, London, 1999.
[8] A. Gentile, A. Mesina, On the continuous wavelet transforms applied to discreet vibrational data for detecting open cracks in damaged beams, International Journal of Solids and Structures, 40 (2003) 259-315.
[9] V. Pakrashi, A. O'Conner, B. Basu, A study on the effects of damage models and wavelet bases for damage identification and calibration in beams, Computer-Aided Civil and Infrastructure Engineering, 22 (2007) 555-569.
[10] H. Kim, H. Melhiem, Damage detection of structures by wavelet analysis, Engineering Structures, 26 (2004) 347-362.
[11] M. M. Reda Taha, A. Noureldin, J.L. Lucero, T.J.Baca, Wavelet transform for structural health monitoring: a compendium of uses and features, Structural Health Monitoring, 5(3), (2006) 267-295.
[12] A. Chukwujekwu Oakafor, A. Dutta, Structural damage detection in beams by wavelet transforms, Smart Materials and Structures, 9 (2000) 906-917.
[13] S. Douka, S. Loutridis, A. Trochidis, Crack identification in beams using wavelet analysis, International Journal of Solids and Structures, 40 (2003) 3557-3569.
[14] S. Douka, S. Loutridis, A. Trochidis, Crack identification in plates using wavelet analysis, Journal of Sound and Vibration, 270 (2004) 279-295.
[15] M. Rucka, K. Wilde, Application of continuous wavelet transform in vibration based damage detection method for beams and plates, Journal of Sound and Vibration, 297 (2006) 536-550.

[16] Y. Huang, D. Meyer, S. Nemat-Nasser, Damage detection with spatially distributed 2D continuous wavelet transform, Mechanics of Materials, 41 (2009) 1097-1107.
[17] Z. Sun, C.C. Chang, Structural damage assessment based on wavelet packet transform, Journal of Structural Engineering, 128(10) (2002) 1354-1361.
[18] M. M. Reda Taha, A. Noureldin, A. Osman, N. El-Sheimy, Introduction to the use of wavelet multiresolution analysis for intelligent structural health monitoring, Canadian Journal of Civil Engineering, 31 (2004) 719-731.
[19] M. M. Reda Taha, A neural-wavelet technique for damage identification in the ASCE benchmark structure using phase II experimental data, Advances in Civil Engineering, 2010(675927) (2010) 1-13.
[20] M. Azarbayejani, A. I. El-Osery, M. M. Reda Taha, Entropy based optimal sensor networks for structural health monitoring of a cable stayed bridge, Smart Materials and Structures 5(4) (2009) 369-379.
[21] J.-C. Hong, Y.Y. Kim, H.C. Lee, Y.W. Lee, Damage detection using Lipschitz exponent estimated by the wavelet transform: applications to vibration modes of a beam, International Journal of Solids and Structures, 39 (2002) 1803-1816.
[22] C.J. Lu, Y.T. Hsu, Vibration analysis of an inhomogeneous string for damage detection by wavelet transform, International Journal of Mechanical Sciences, 44 (2002) 745-754.
[23] Y.W. Kwon, H. Bang, The finite element method using matlab, second ed. CRC Press, 2000, pp. 237-244.
[24] A.D. Dimarogonas, Vibration of cracked structures: a state of the art review, Engineering Fracture Mechanics, 55 (1996) 831-857.
[25] W. Ostachowicz, M. Krawczuk, On modeling of structural stiffness loss due to damage. DAMAS 2001, 4th International Conference on Damage Assessment of Structures, Cardiff, (2001) 185-199.
[26] M.A. Mahmoud, Effect of cracks on the dynamic response of a simple beam subject to a moving load, Proceedings of the Institute of Mechanical Engineers, Part F: Journal of Rail and Transit, 15 (2001) 207-215.
[27] H. Tada, P.C. Paris, G.R. Irwin, The Stress Analysis of Cracks Handbook, ASME Press, New York, 2000.
[28] C.P. Ratcliffe, Damage detection using a modified Laplacian operator on mode shape data, Journal of Sound and Vibration, 204(3) (1997) 505-517.
[29] S.H.S. Carneiro, D.J. Inman, Continuous model for the transverse vibration of cracked Timoshenko beams, Transactions of the ASME, Journal of Vibration and Acoustics, 124 (2002) 310-320.
[30] S. Christides, D.S. Barr, One-dimensional theory of cracked Bernoulli-Euler beams, International Journal of Mechanical Science, 26 (1984) 639-648.
[31] J.W. Tedesco, W.G. McDougal, C.A. Ross, Structural Dynamics: Theory and Applications, Addison Wesley Longman, Inc., Menlo Park CA, 1999.
[32] Z. Zhou, H. Adeli, Wavelet energy spectrum for time-frequency localization of earthquake energy, International journal of Imaging systems and Technology, 13 (2003) 133-140.
[33] Y.B. Yang, J.D. Yau, Y.S. Wu, Vehicle-Bridge Interaction Dynamics with Applications to High Speed Railways. World Scientific Publishing Company, Singapore, 2004.

[34] M.F. Green, D. Cebon, Dynamic interaction between heavy vehicles and highway bridges, Computers and Structures, 62(2) (1997) 253-264.
[35] F. Yang, G.A. Fonder, An iterative solution method for dynamic response of bridge-vehicle systems, Earthquake Engineering and Structural Dynamics, 25 (1996) 195-215.
[36] L. Frýba, Vibration of solids and structures under moving Loads, 3rd ed., Thomas Telford, London, 1999.
[37] M.M. El-Madany, Design optimization of truck suspension using covariance analysis, Computers and Structures, 28(2) (1988) 241-246.
[38] N.K. Harris, E.J. OBrien, A. González, Reduction of bridge dynamic amplification through adjustment of vehicle suspension damping. Journal of Sound and Vibration, 302 (2007) 471-485.
[39] D. Cebon, Handbook of Vehicle-Road Interaction, Swets & Zeitlinger, Netherlands, 1999.
[40] C. Torrence, G.P. Compo, A practical guide to wavelet analysis, Bulletin of the American Meteorological Society, 79 (1998) 61-78.
[41] S. D. Meyers, B. G. Kelly, J.J. O'Brien, An introduction to wavelet analysis in oceanography and meteorology: With application to the dispersion of Yanai waves, Monthly Weather Review, 121 **(**1993) 2858–2866.

Figure Captions
Click here to view linked References

Fig. 1 Mid-span acceleration of a 40 m bridge traversed by a constant load moving at 3 m/s.

Fig. 2 Wavelet transform of the healthy signal shown in Fig. 1.

Fig. 3 Wavelet transform of the damaged acceleration signal shown in Fig. 1.

Fig. 4 Coefficient line plot for the healthy and damaged signals shown in Fig. 1.

Fig. 5 Sketch of beam discretized model subject to a moving force.

Fig. 6 Corrupted mid-span acceleration signal of healthy and damaged bridges.

Fig. 7 Coefficient line plot of acceleration signal for crack at the one third point: (a) delta = 0.3 (b) delta = 0.1.

Fig. 8 Vertical sections through wavelet transform surface: (a) Wavelet transform surface when delta = 0.2 at the 1/3 point, (b) Absolute value of wavelet coefficients for vertical sections at different positions of the moving load, (c) Absolute value of wavelet coefficients at different positions of the moving load for scale range between 500 and 1200.

Fig. 9 Sketch showing strip C of the 3D wavelet surface.

Fig. 10 Total wavelet energy content associated with different strips when delta = 0.1 at 1/3 point.

Fig. 11 Relative energy associated with different strips for a healthy condition (delta = 0.0) and a low level of damage (delta = 0.1).

Fig. 12 Relative energy for bridge acceleration signal simulated at three locations simultaneously and average of the three locations.

Fig. 13 Average relative energy when acceleration simulated at 3 locations simultaneously for different damage levels.

Fig. 14 Average relative energy when acceleration signals from a 10 m bridge were analyzed between scales of 140 and 425.

Fig. 15 Average relative energy when acceleration signals from a 20 m bridge were analyzed between scales of 230 and 680.

Fig. 16 Damped and undamped mid-span acceleration signals for healthy bridge.

Fig. 17 Average relative energy when damped acceleration simulated at 3 locations simultaneously for different damage levels.

Fig. 18 Average relative energy for different damage levels when the acceleration signal contains 10% noise and are simulated with a damping ratio $\xi = 0.04$.

Fig. 19 Average relative energy when acceleration simulated at 3 locations simultaneously for bridge with 2 damages.

Fig. 20 Mid-span acceleration signal of bridge damaged at the one 1/3 point (delta = 0.3).

Fig. 21 Wavelet transform of signal shown in Fig. 17: (a) scales 1-1500, (b) scales 500-1500.

Fig. 22 Wavelet transform of shortened acceleration signal.

Fig. 23 Shortened signal padded at both ends.

Fig. 24 Wavelet transform of signal shown in Fig. 20.

Fig. 25 Average relative energy for various damage levels at different locations (smooth road profile, speed = 3 m/s, noise 3%).

Fig. 26: (a) Road profile on the bridge, (b) Mid-span acceleration signal with road profile on bridge including 3% noise.

Fig. 27 Wavelet transform of signal shown in Fig. 23(b) for scales between 1 and 1500.

Fig. 28 Average relative energy for various damage levels at different locations (class 'A' road profile, speed = 3 m/s, 3% noise).

Fig. 29 Average relative energy for various damage levels at different locations (class 'B' road profile, speed = 3 m/s, 3% noise).

Fig. 30 Average relative energy for various damage levels at 0.33L (class 'A' road profile, speed = 7 m/s, 3% noise).

Table 1

Dimensional Data (m)		
	Wheel base	3.78
	Dist from centre of mass to front axle	1.94
	Dist from centre of mass to rear axle	1.84
	Overall length of truck	6.00
Mass and Inertia Parameters		
Mass Parameters (kg)	*Front axle mass*	700
	Rear axle mass	1,100
	Sprung body mass	13,300
Inertia Parameters (kgm^2)	*Pitch moment of inertia of truck*	41,008
Suspension Parameters		
Spring Stiffness (kN/m)	*Front axle*	400
	Rear axle	1,000
Damping Coeffs (kNs/m)	*Front axle*	10
	Rear axle	10
Tyre Stiffness (kN/m)	*Front axle*	1,750
	Rear axle	3,500

Table 1. Parameters for truck model.

Figure 1

Click here to download high resolution image

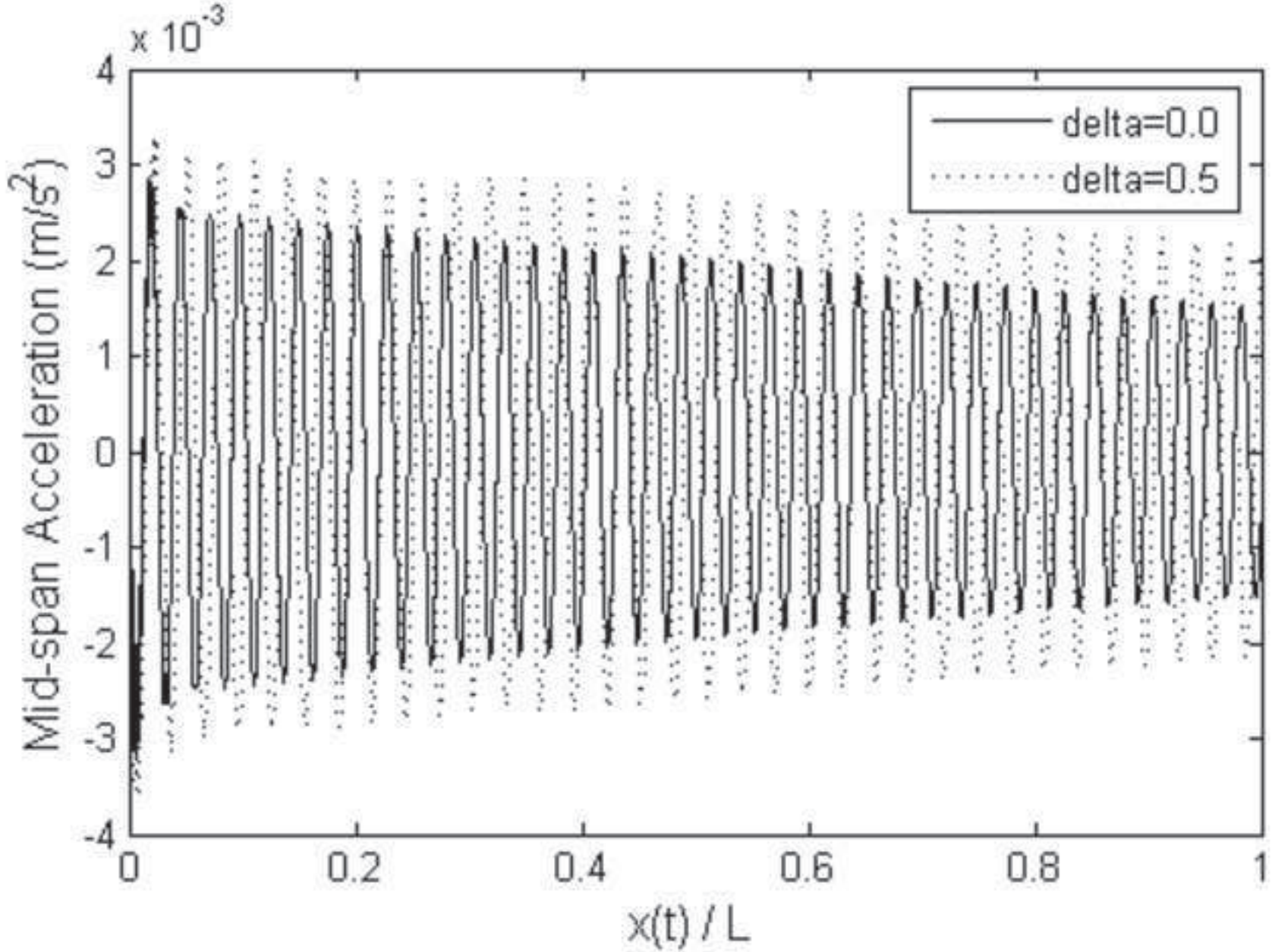

Figure 2

Click here to download high resolution image

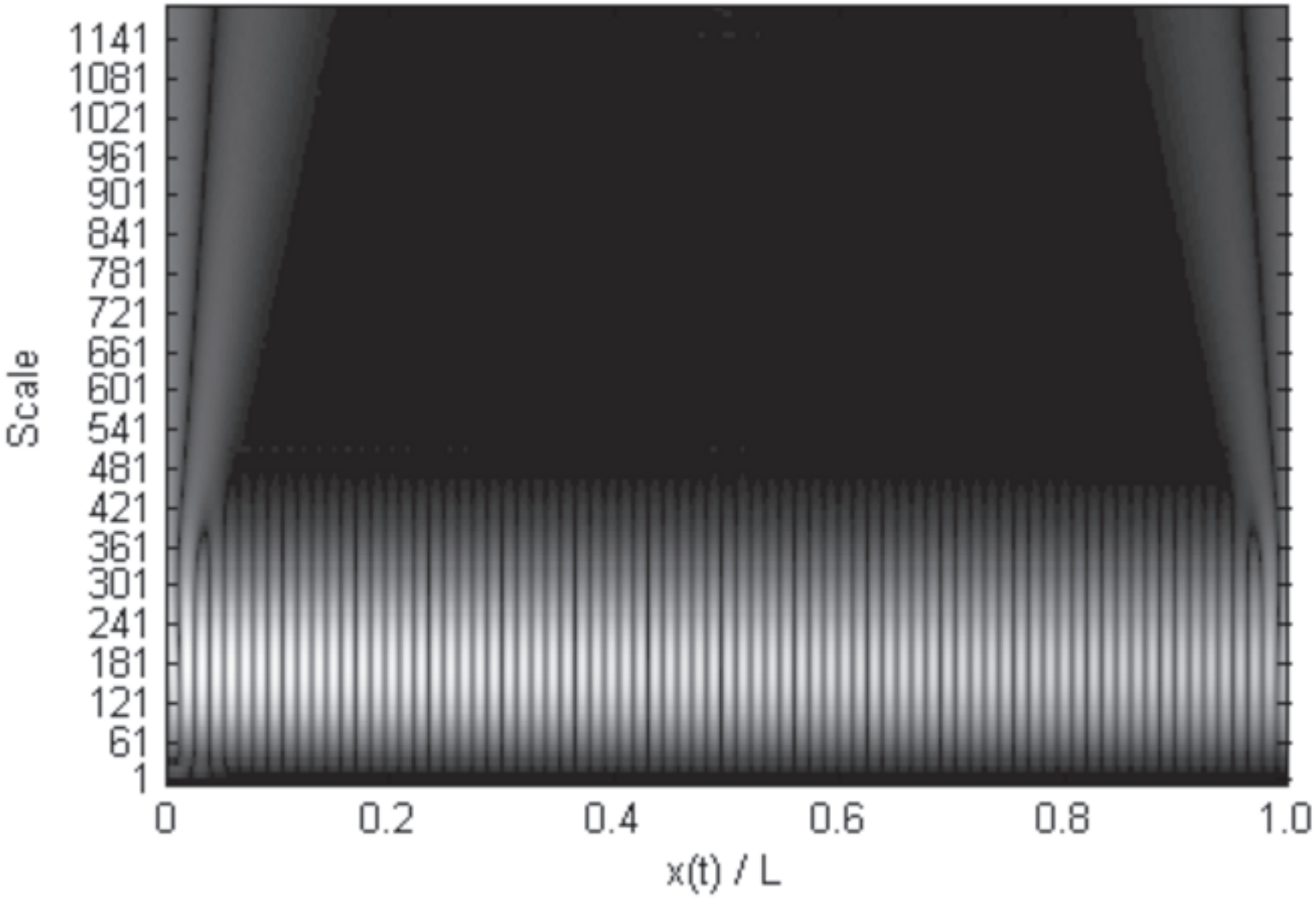

Figure 3

Click here to download high resolution image

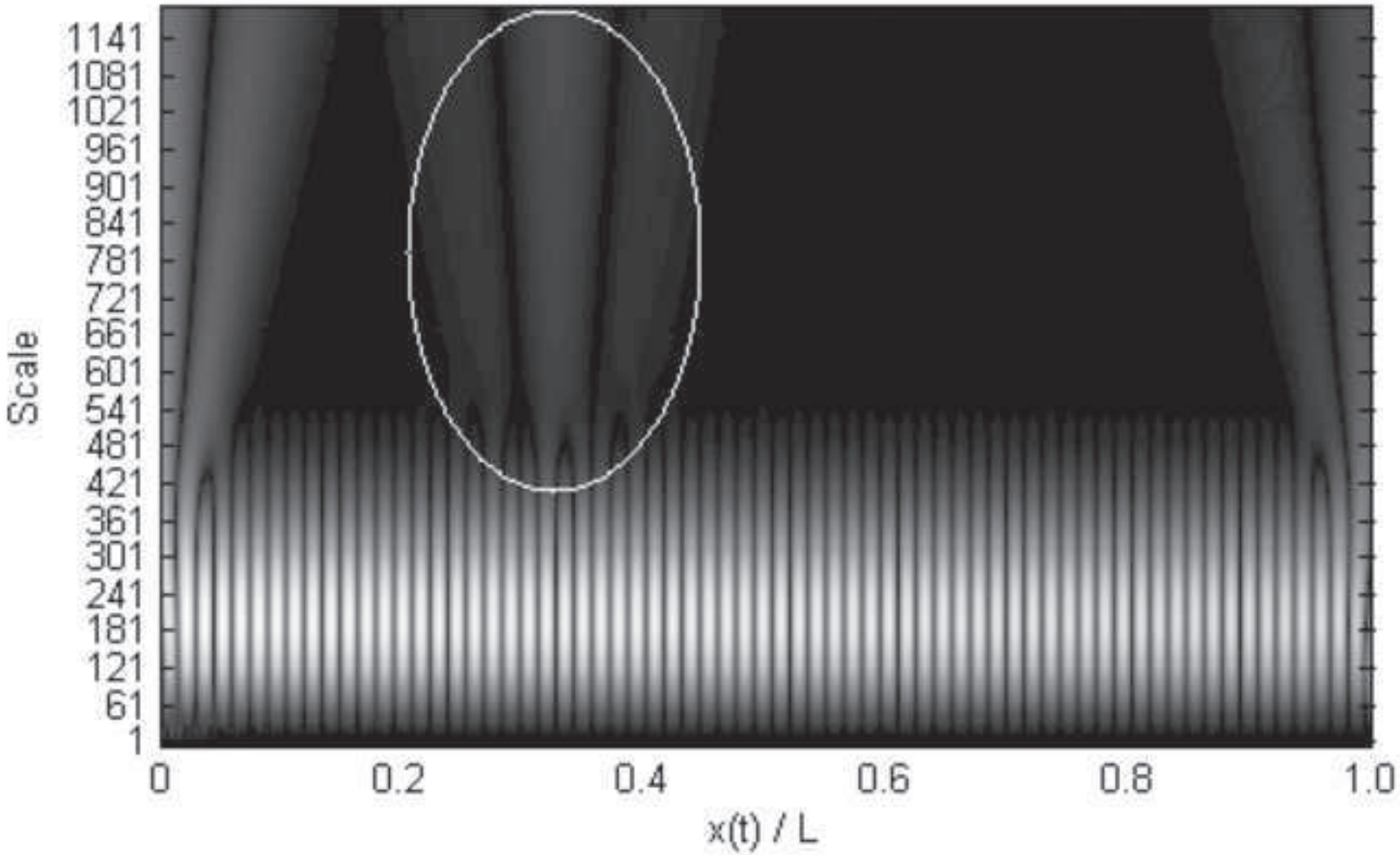

Figure 4

Click here to download high resolution image

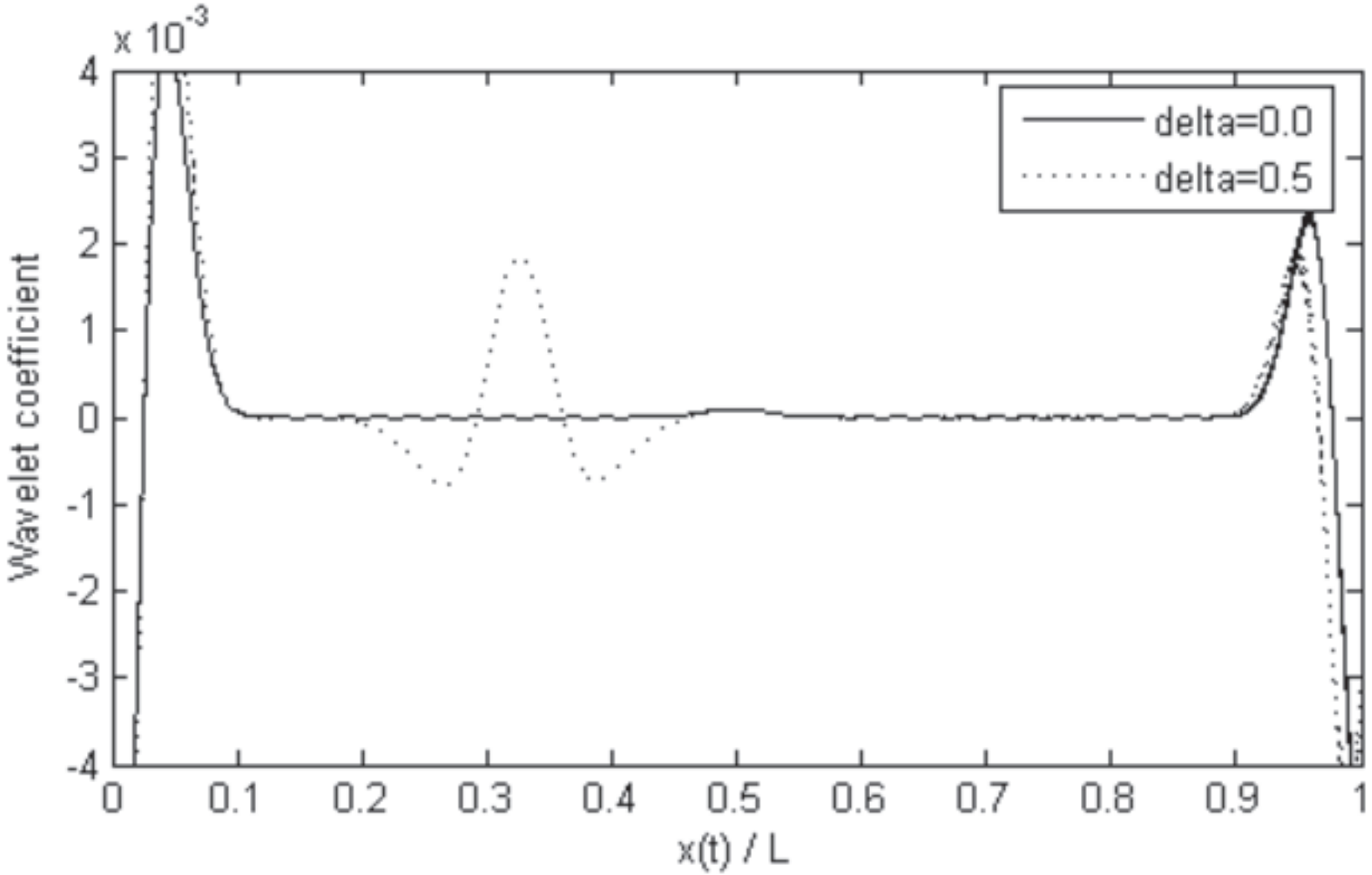

Figure 5

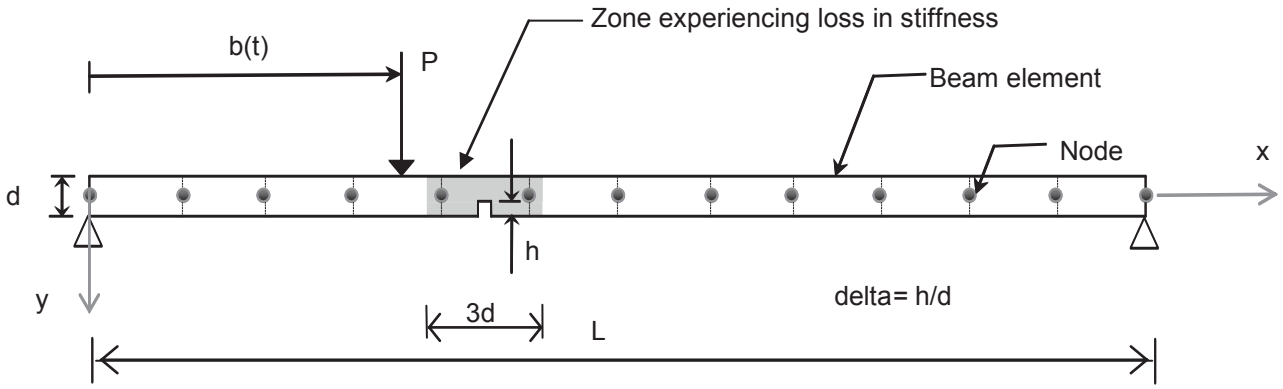

Figure 5 Sketch of beam discretized model subject to a moving force.

Figure 6

Click here to download high resolution image

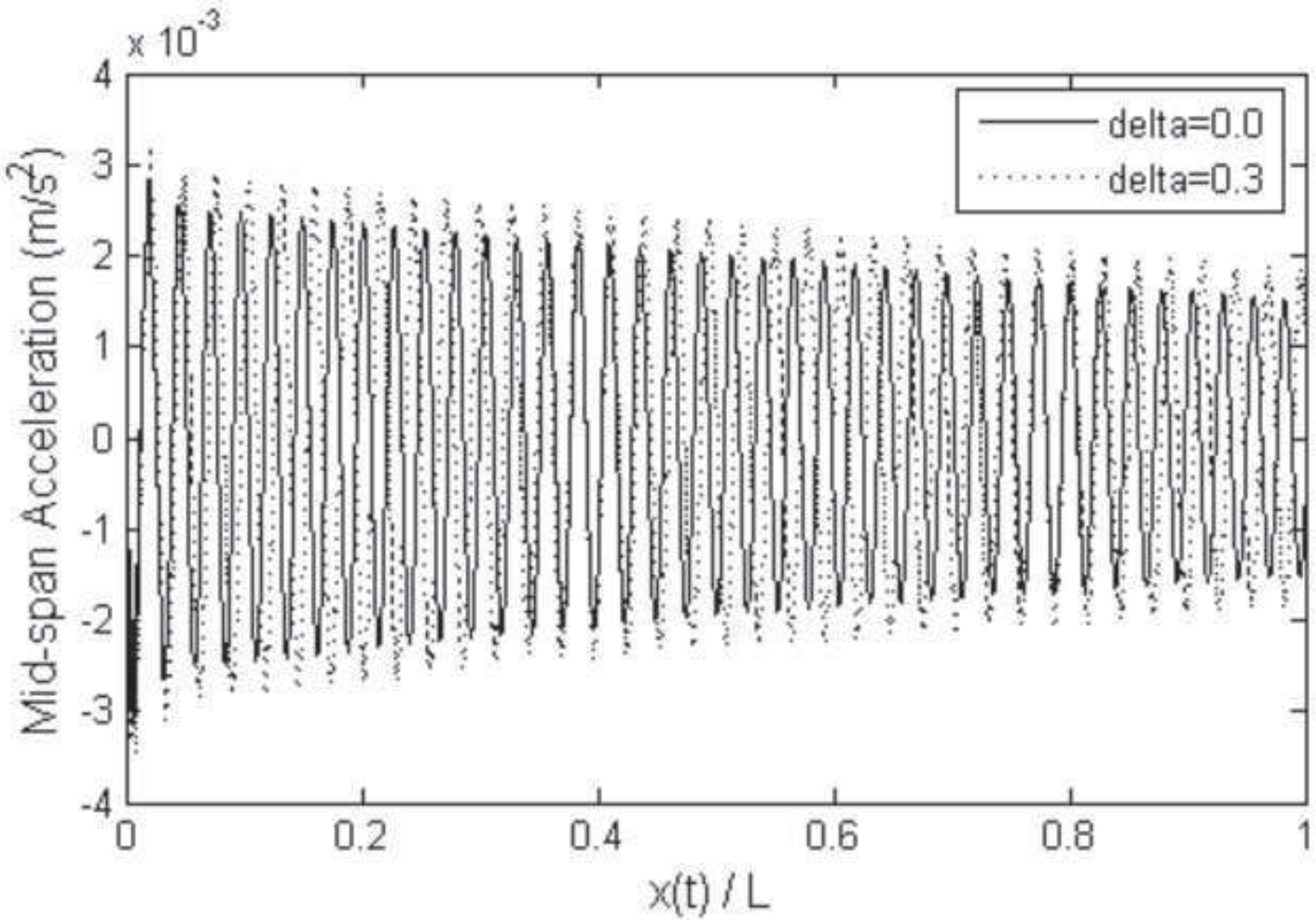

Figure 7
Click here to download high resolution image

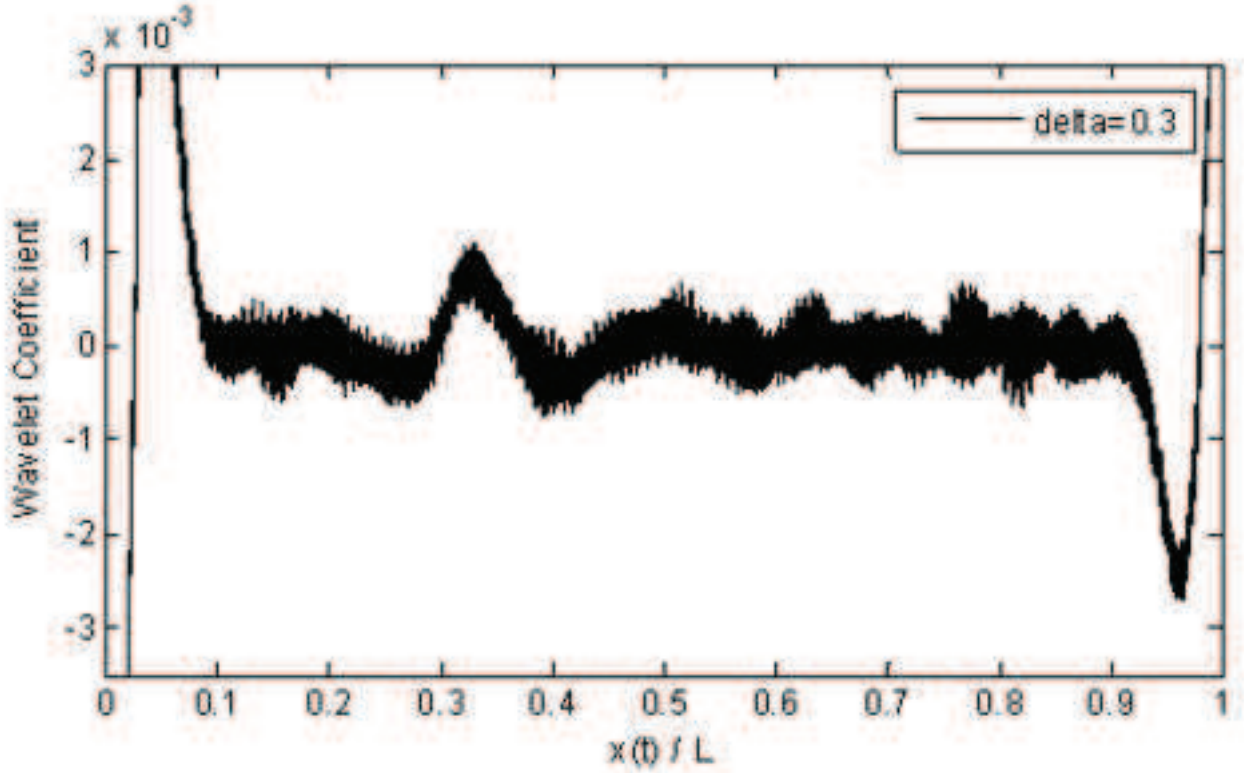

(a)

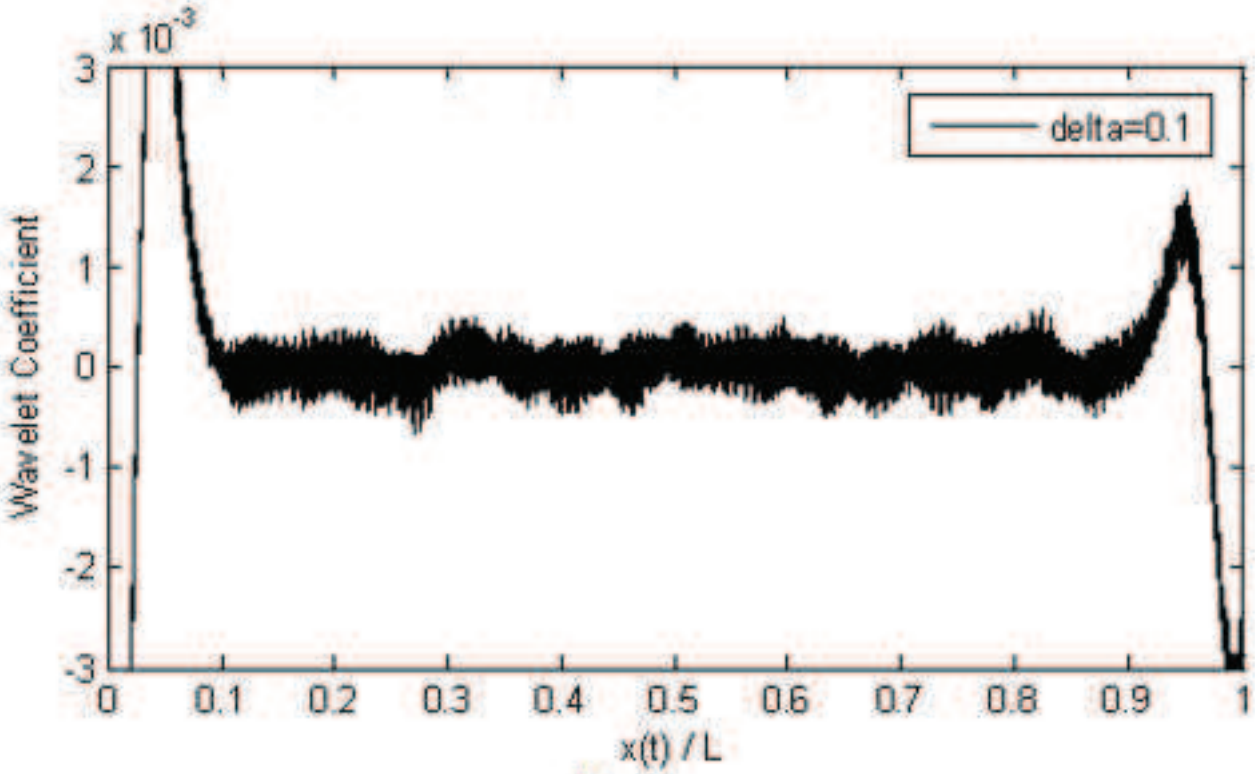

(b)

Figure 8

Click here to download high resolution image

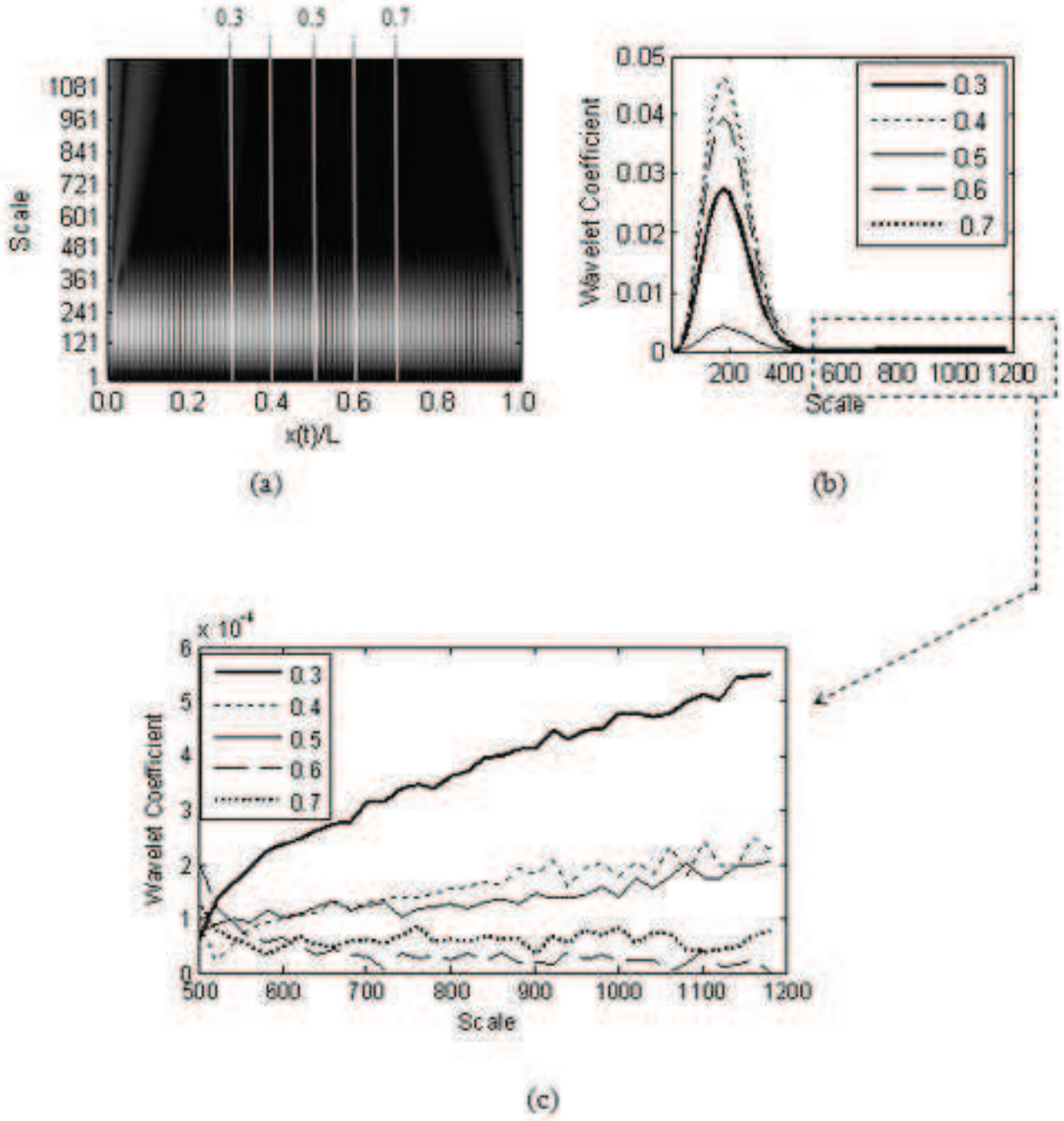

Figure 9

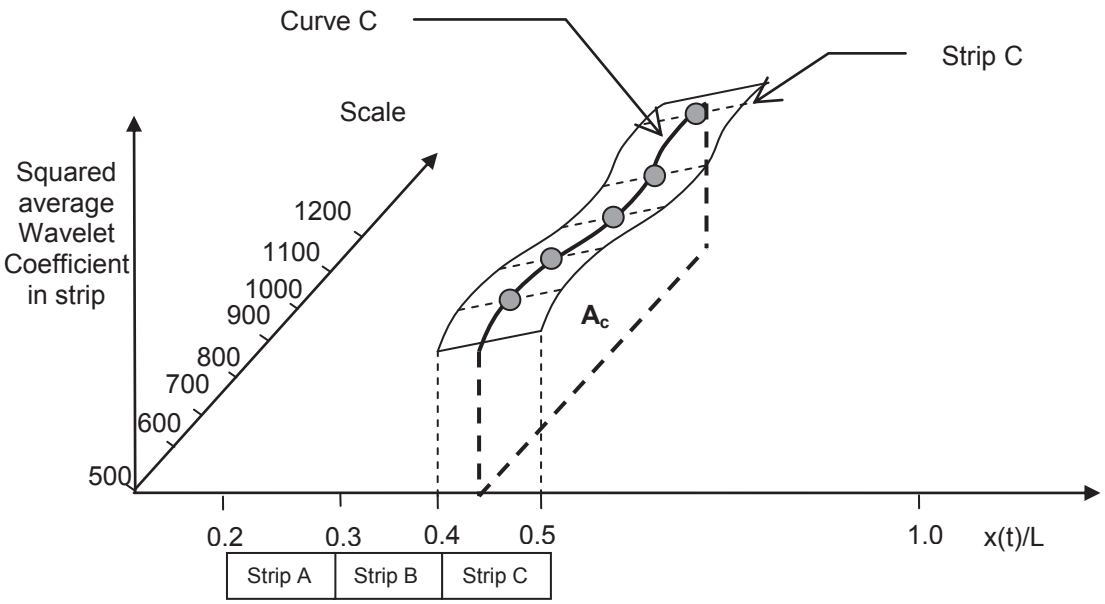

Figure 9 Sketch showing strip C of the 3D wavelet surface.

Figure 10
Click here to download high resolution image

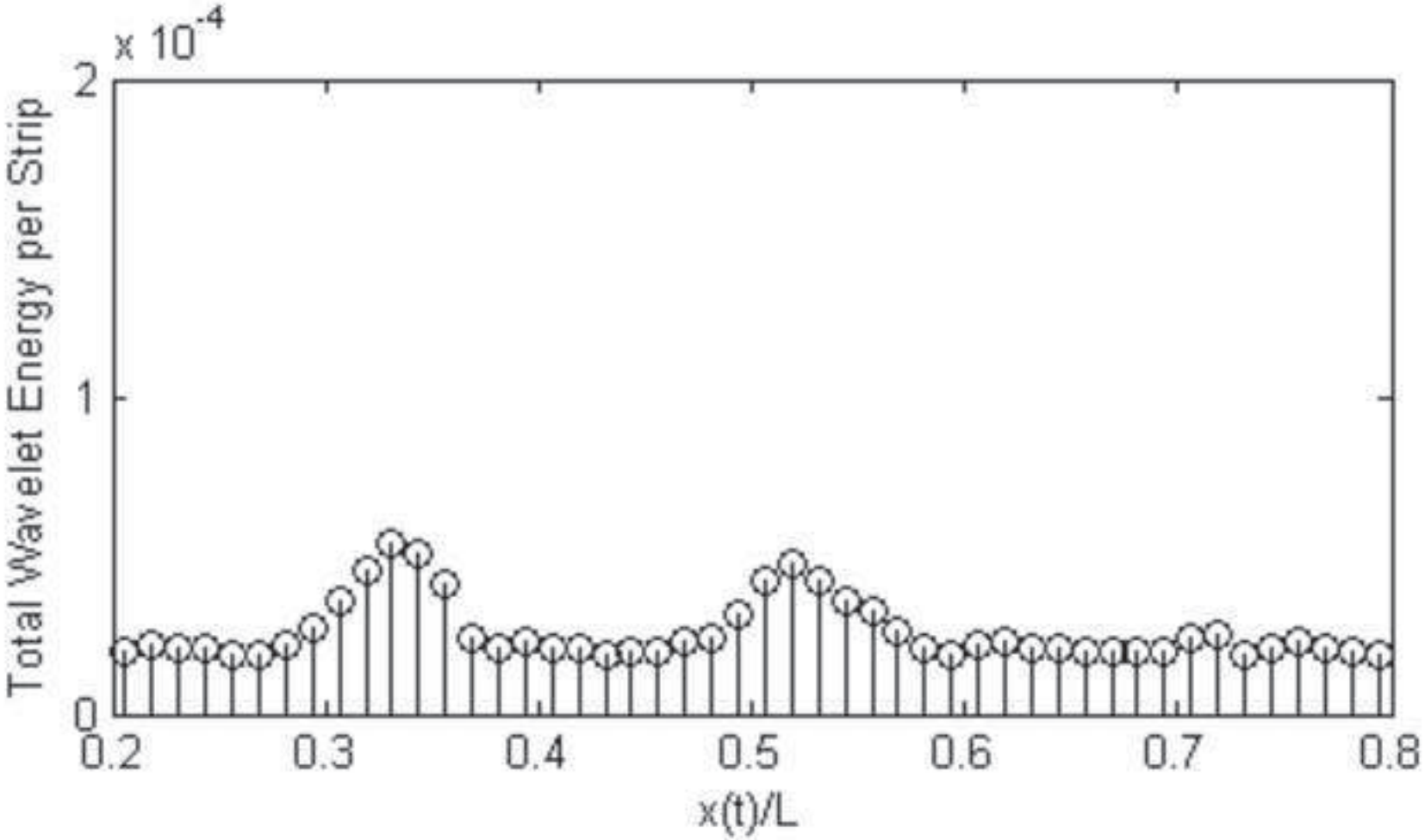

Figure 11
Click here to download high resolution image

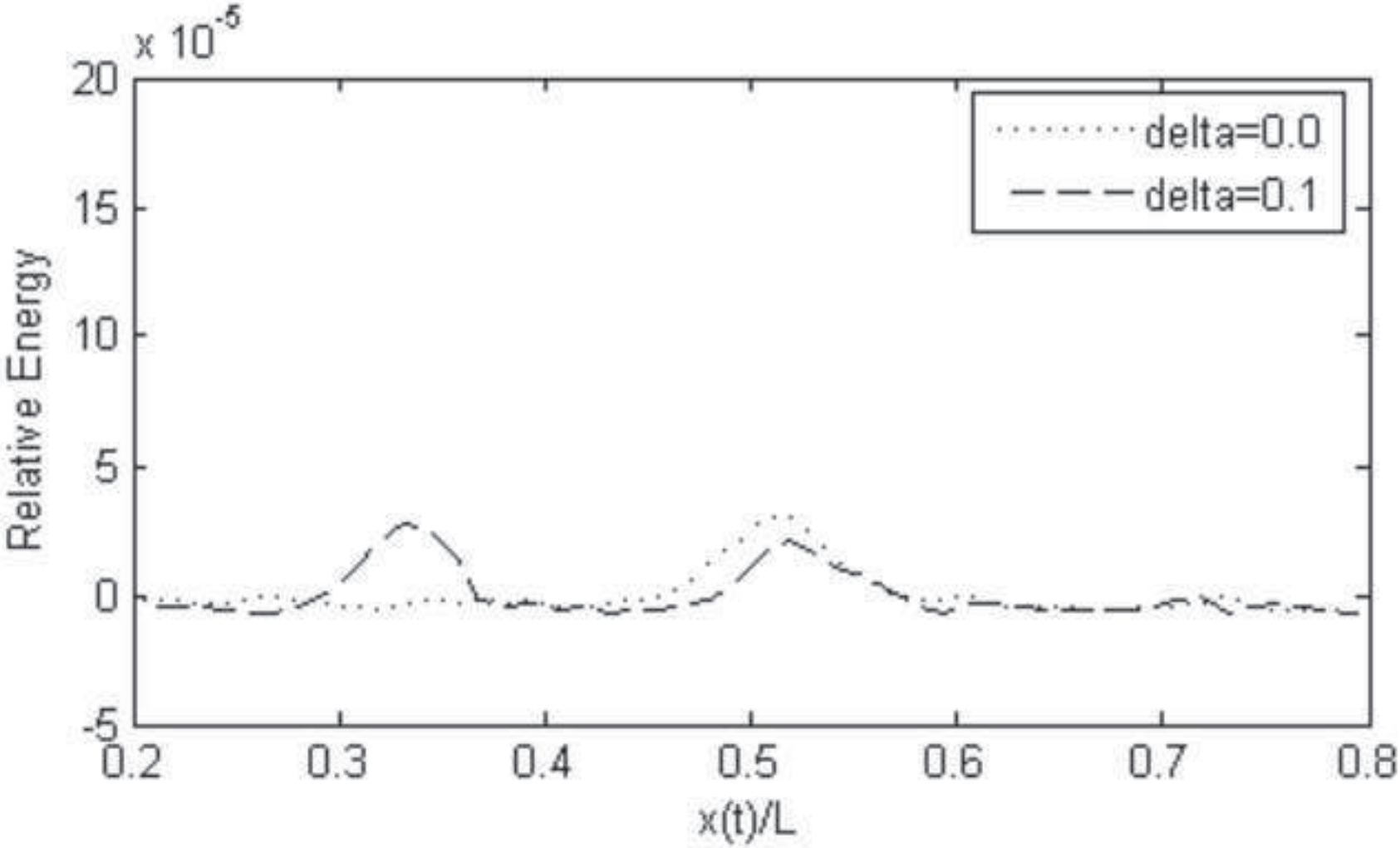

Figure 12

Click here to download high resolution image

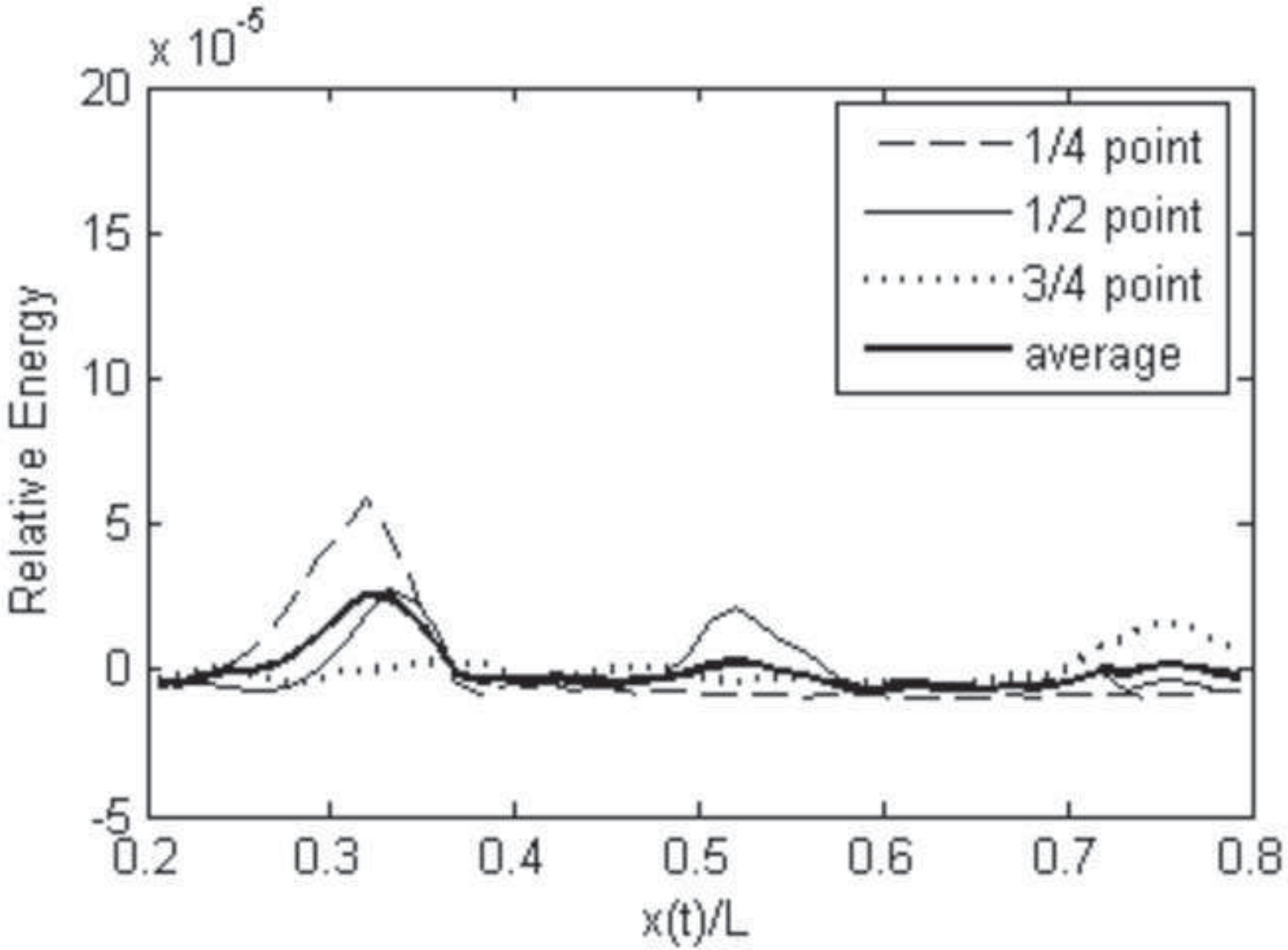

Figure 13
Click here to download high resolution image

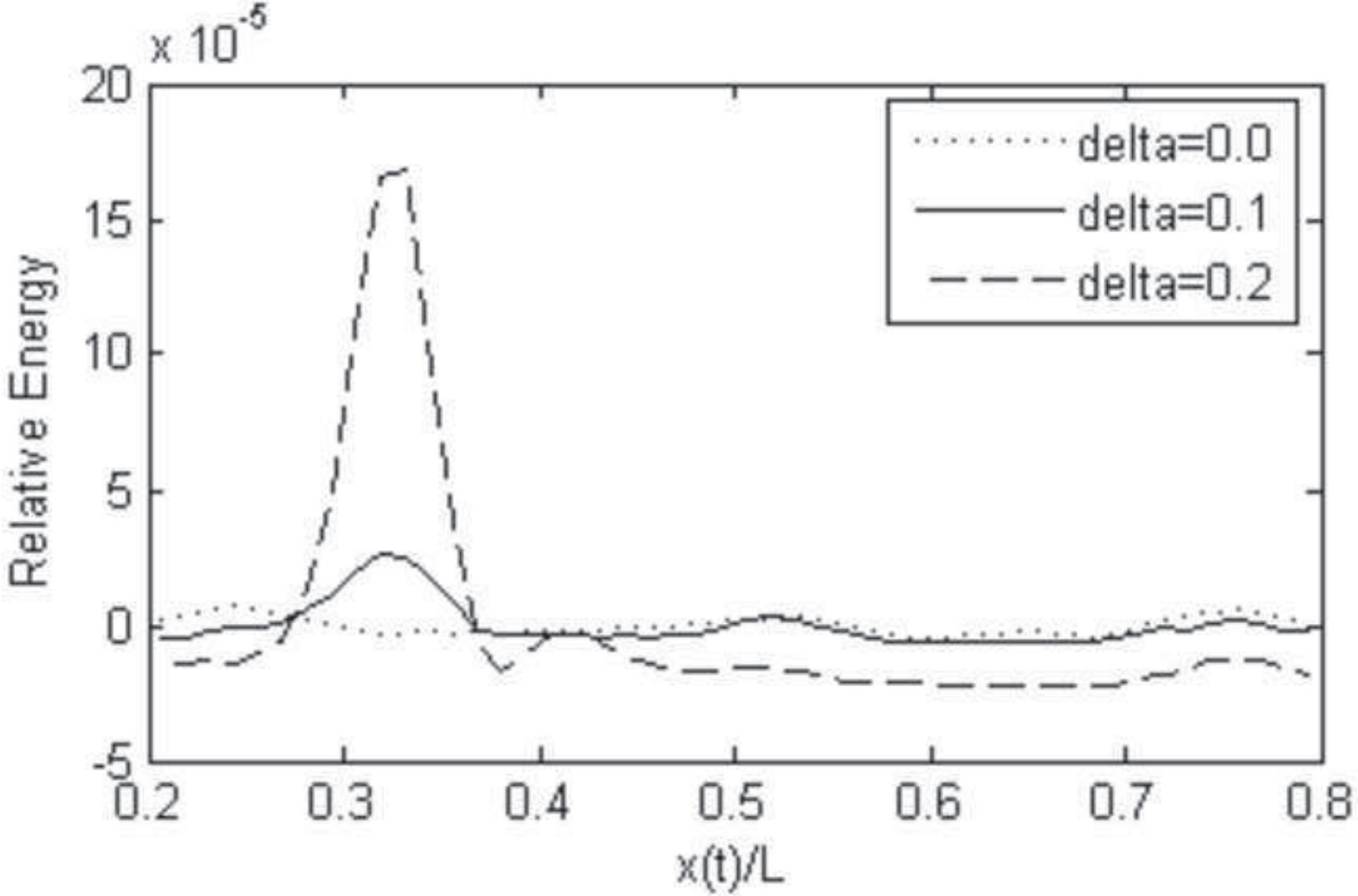

Figure 14

Click here to download high resolution image

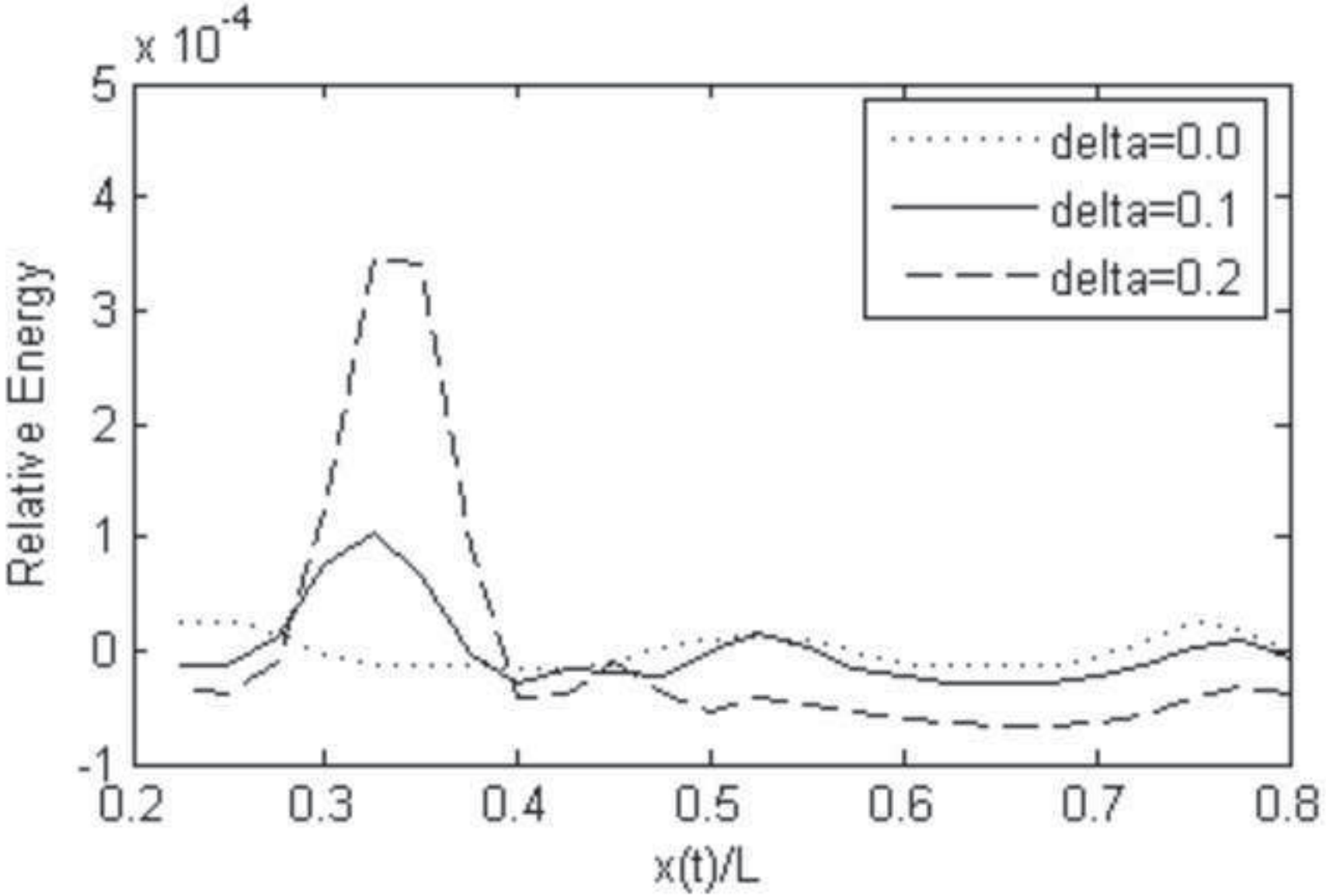

Figure 15

Click here to download high resolution image

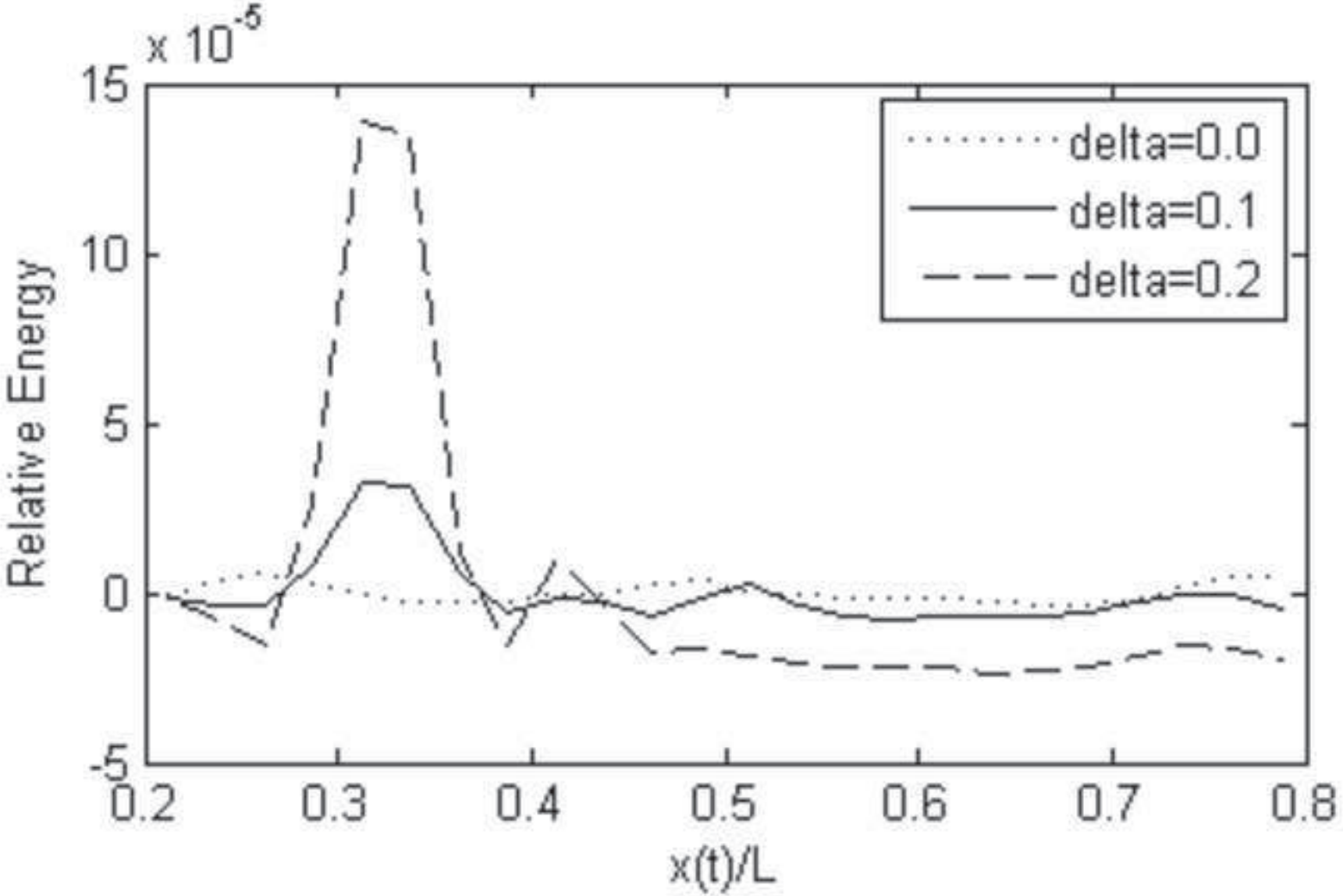

Figure 16
Click here to download high resolution image

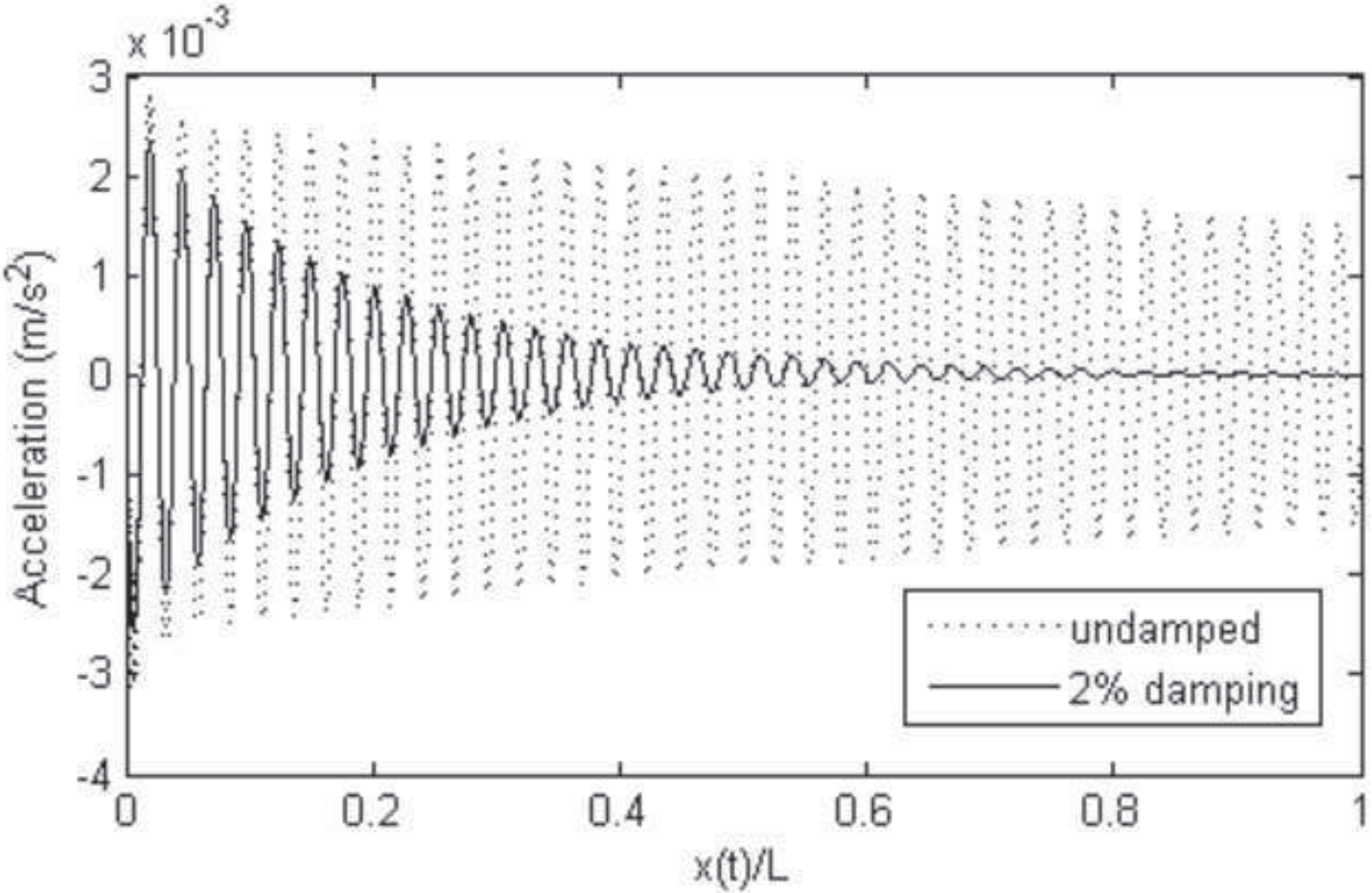

Figure 17

Click here to download high resolution image

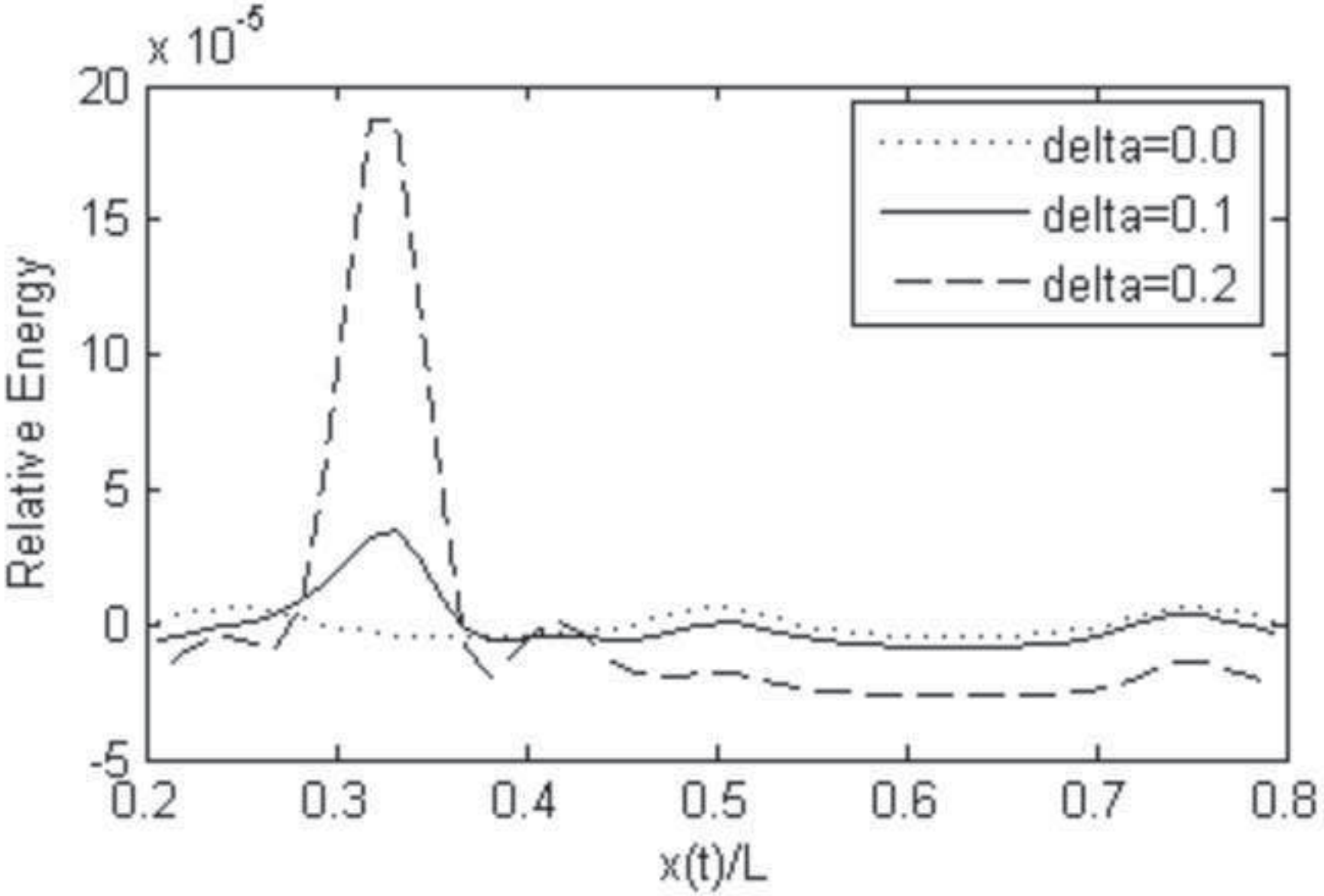

Figure 18
Click here to download high resolution image

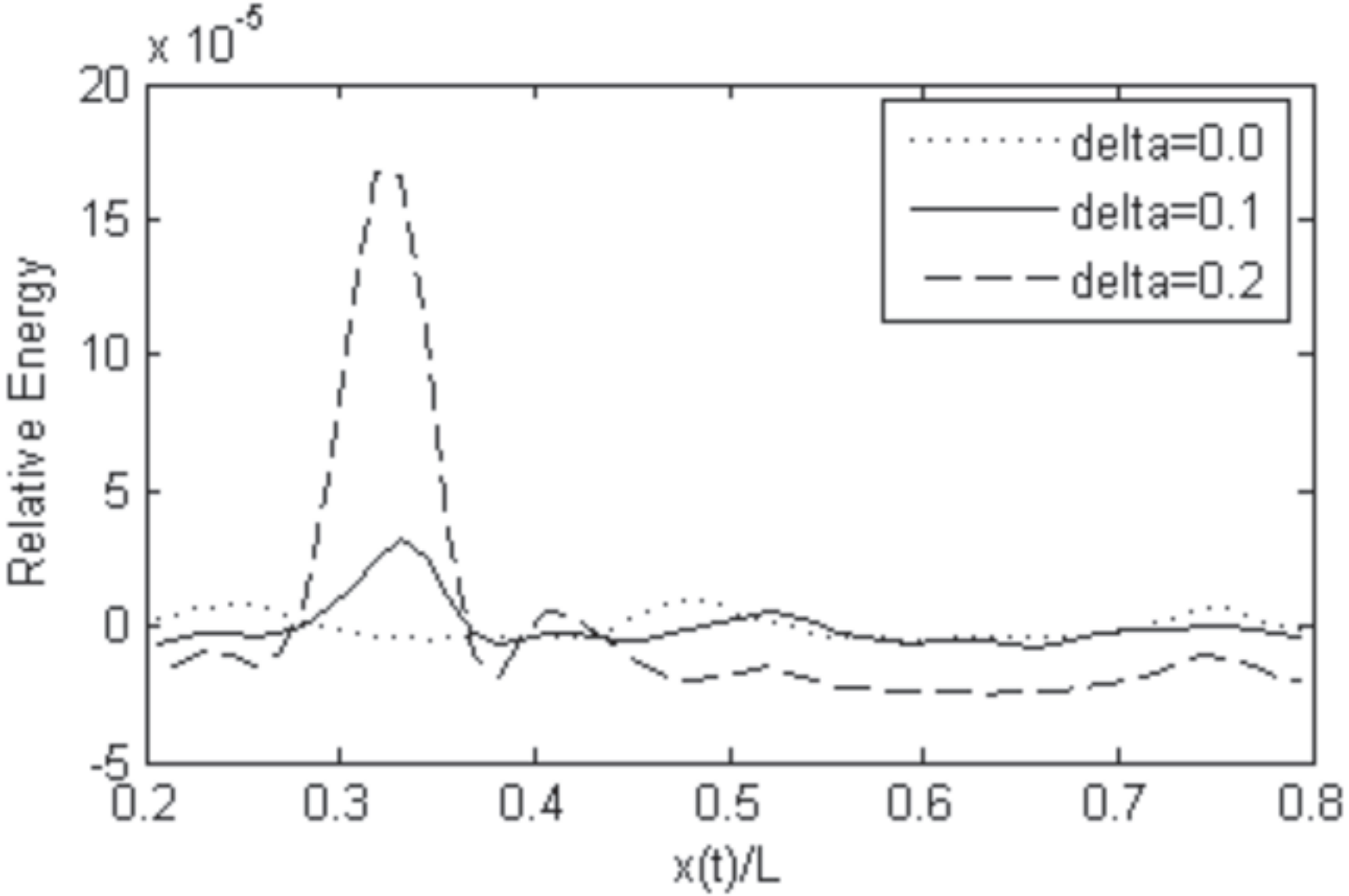

Figure 19
Click here to download high resolution image

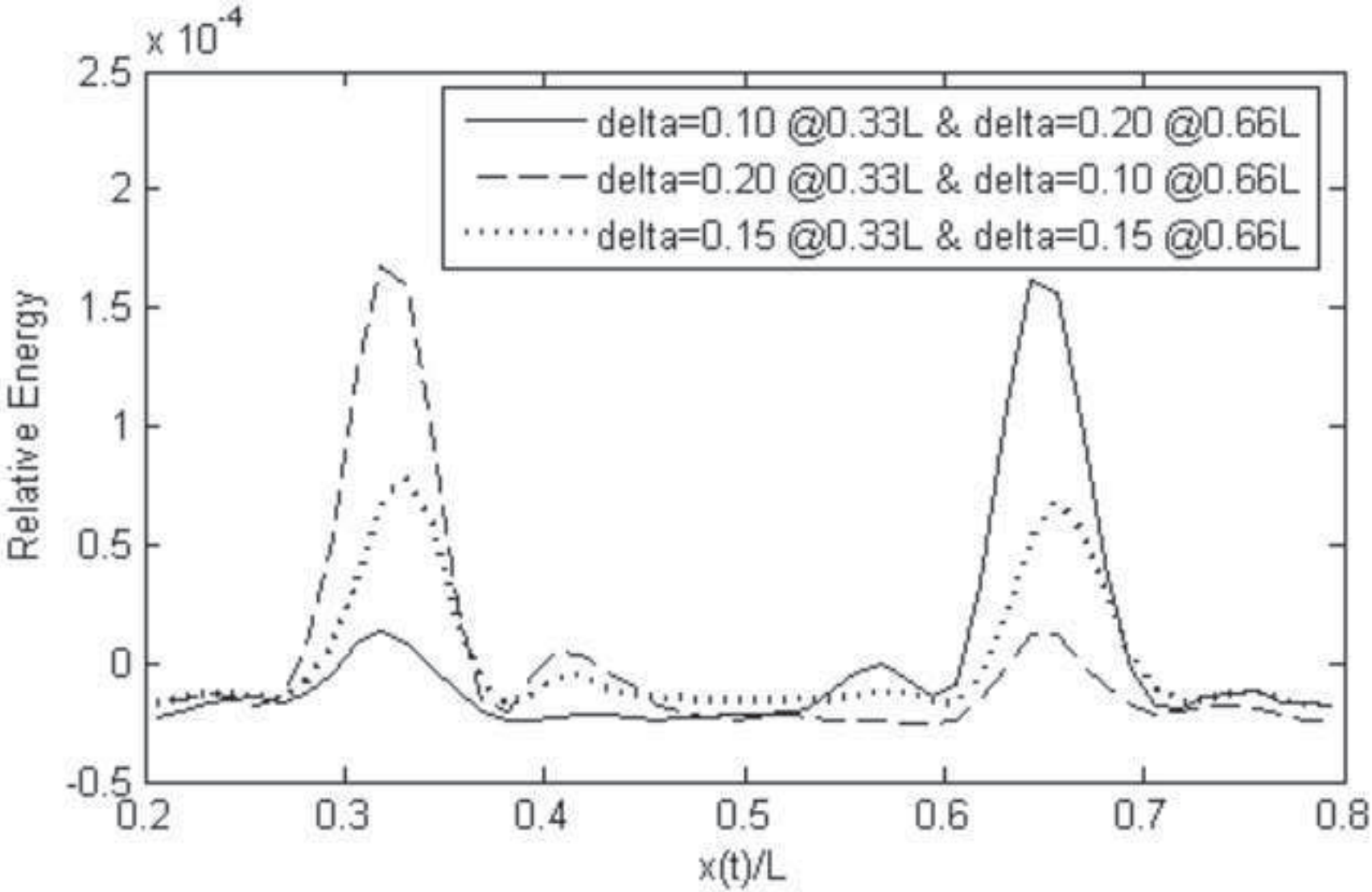

Figure 20

Click here to download high resolution image

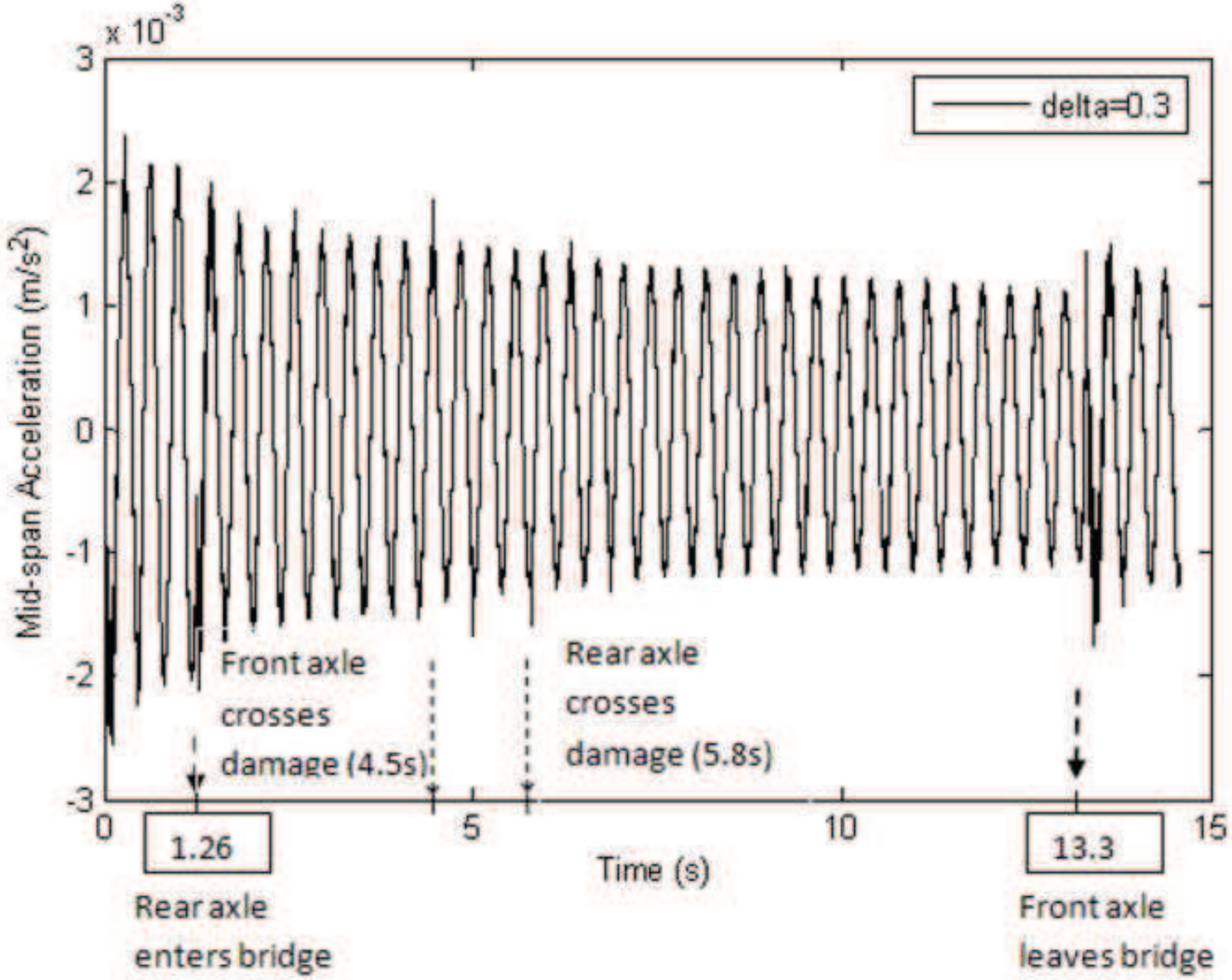

Figure 21
Click here to download high resolution image

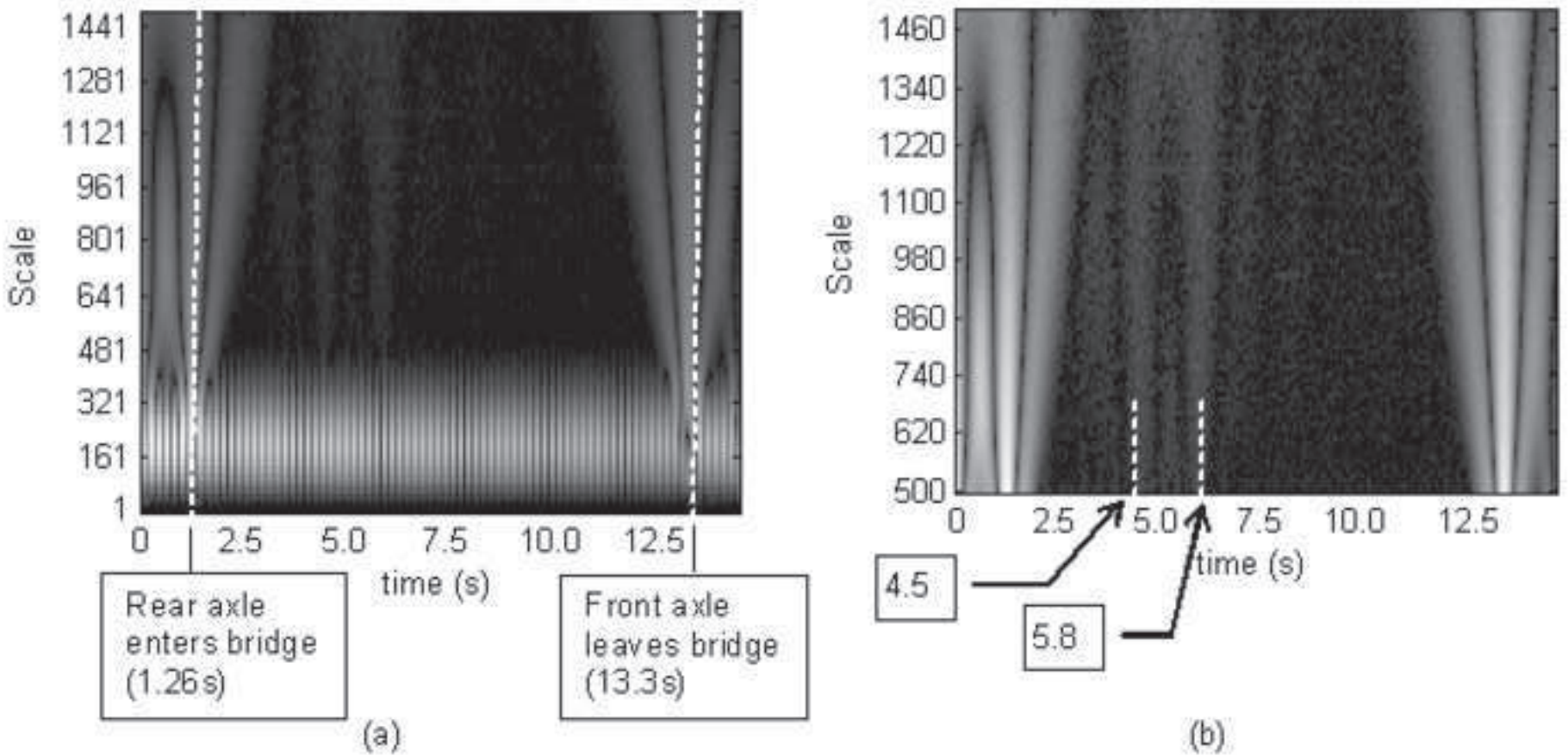

Figure 22
Click here to download high resolution image

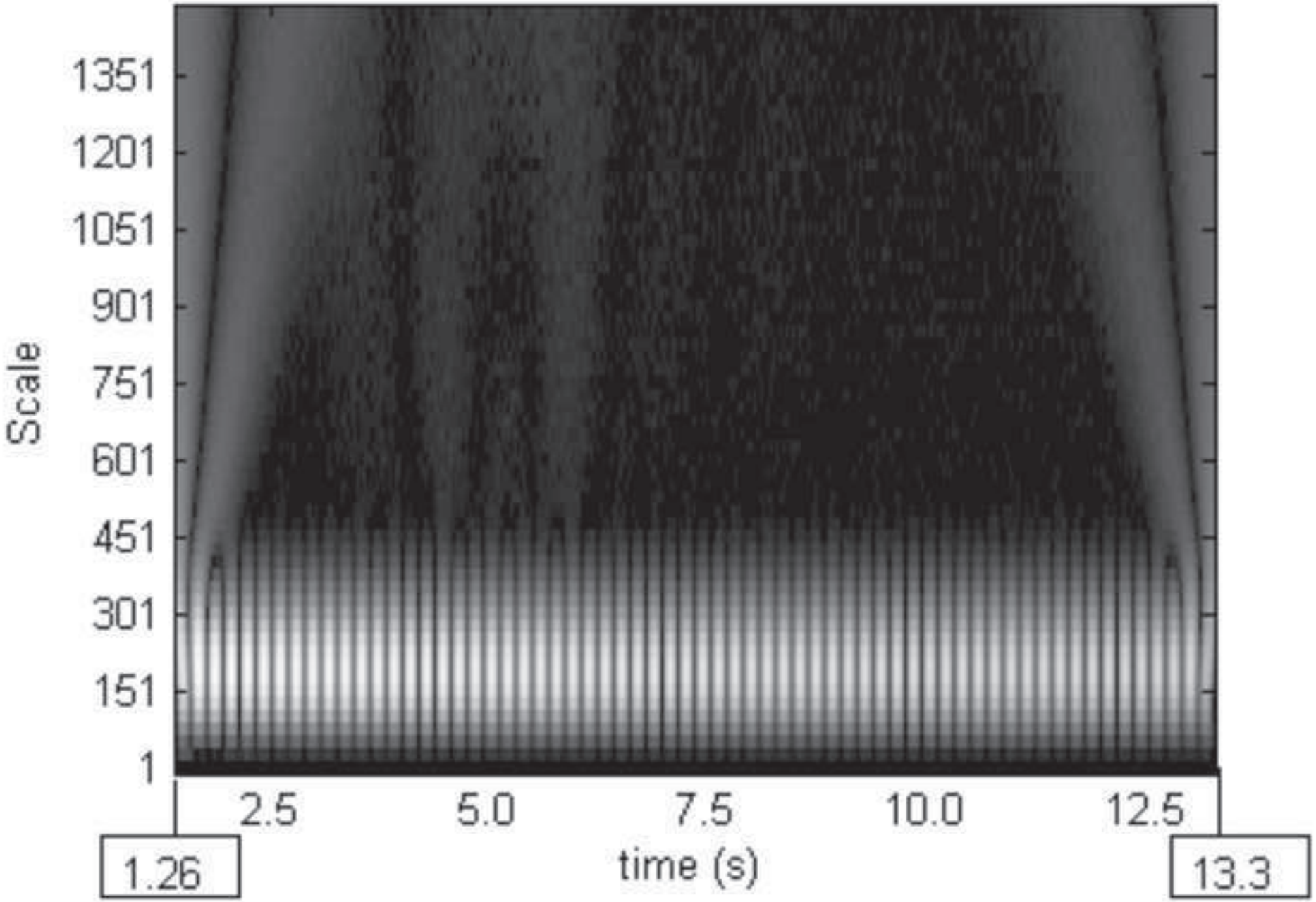

Figure 23
Click here to download high resolution image

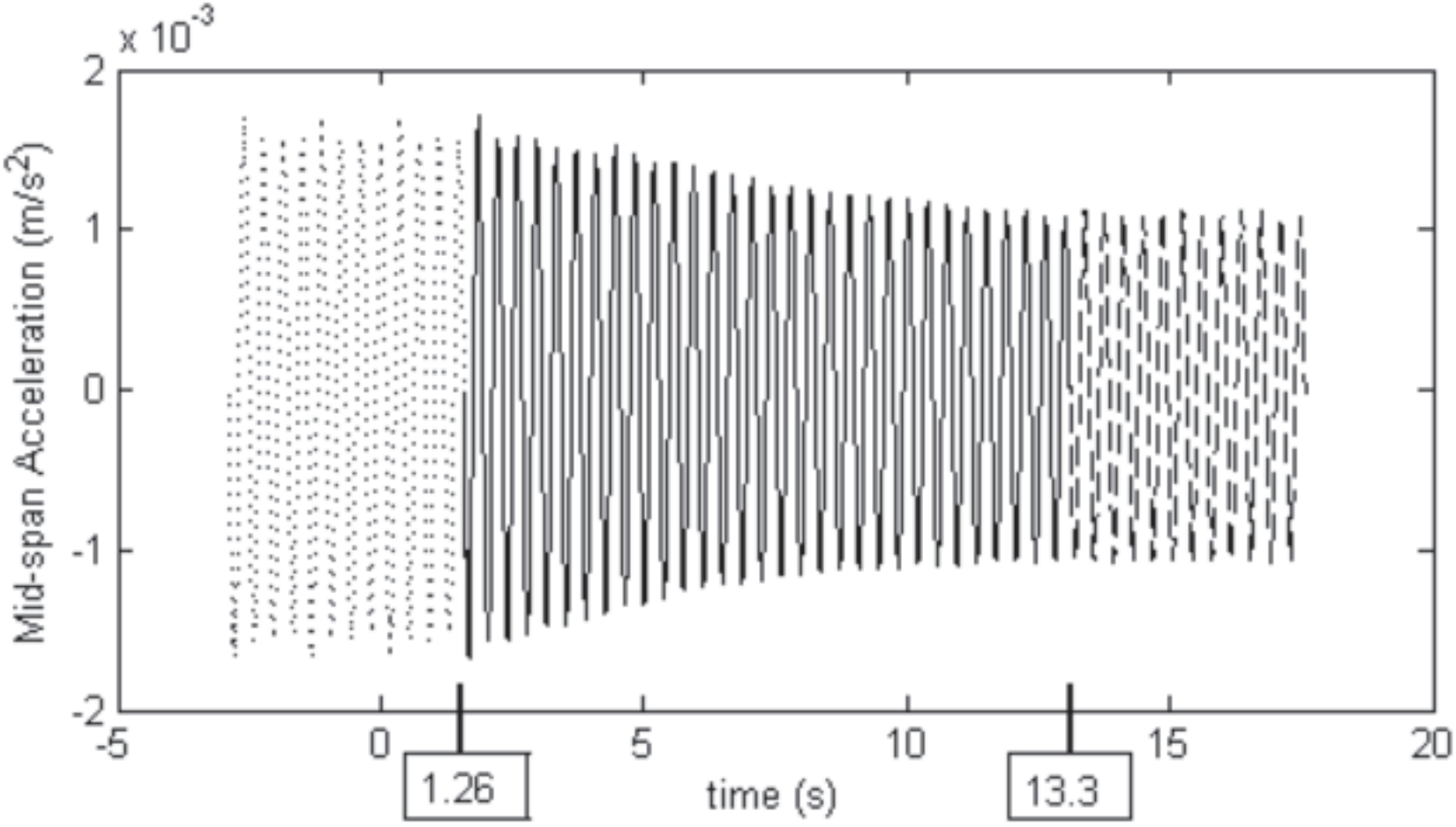

Figure 24

Click here to download high resolution image

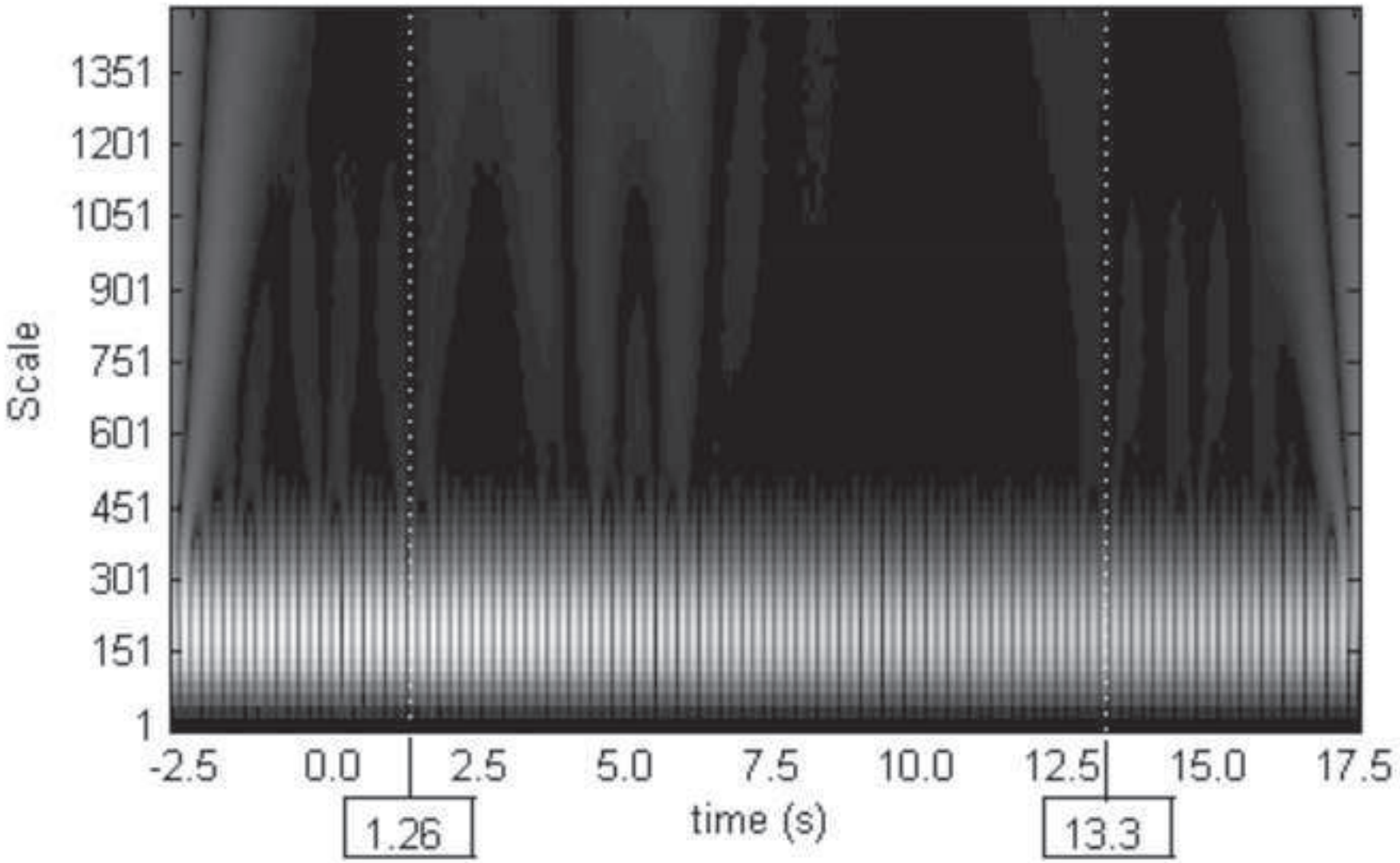

Figure 25
Click here to download high resolution image

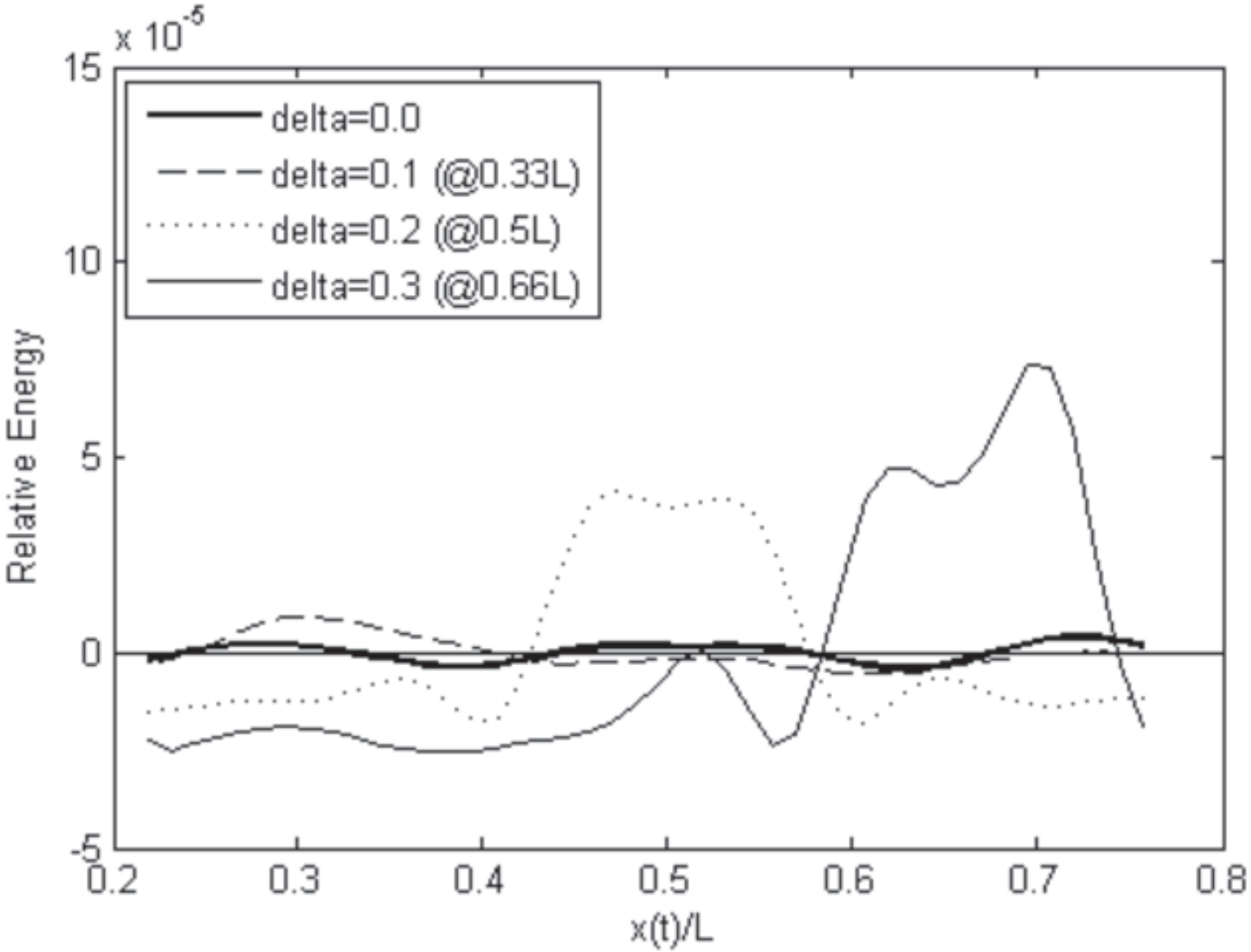

Figure 26
Click here to download high resolution image

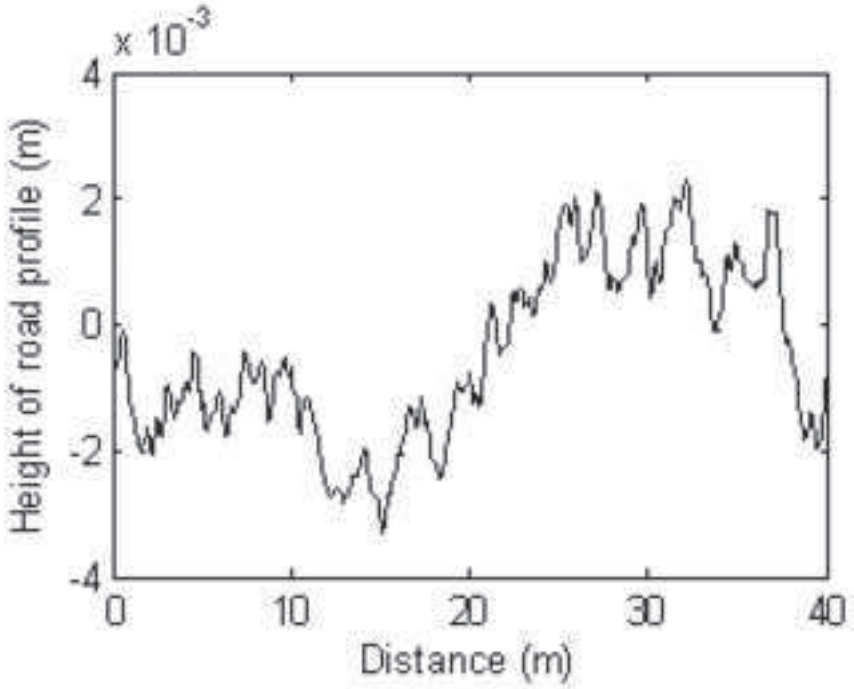

(a)

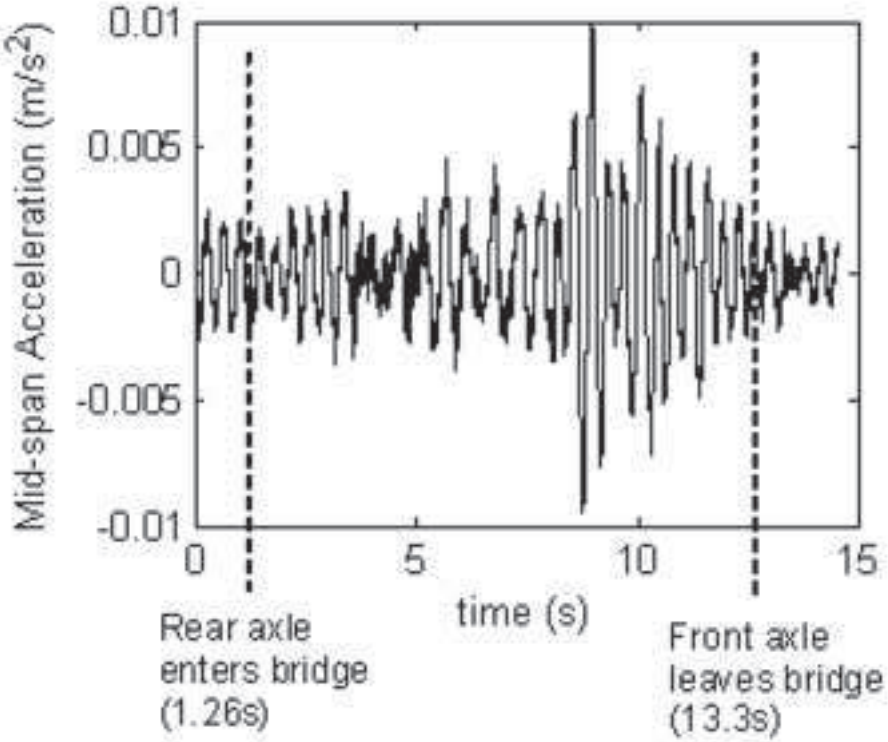

(b)

Figure 27
Click here to download high resolution image

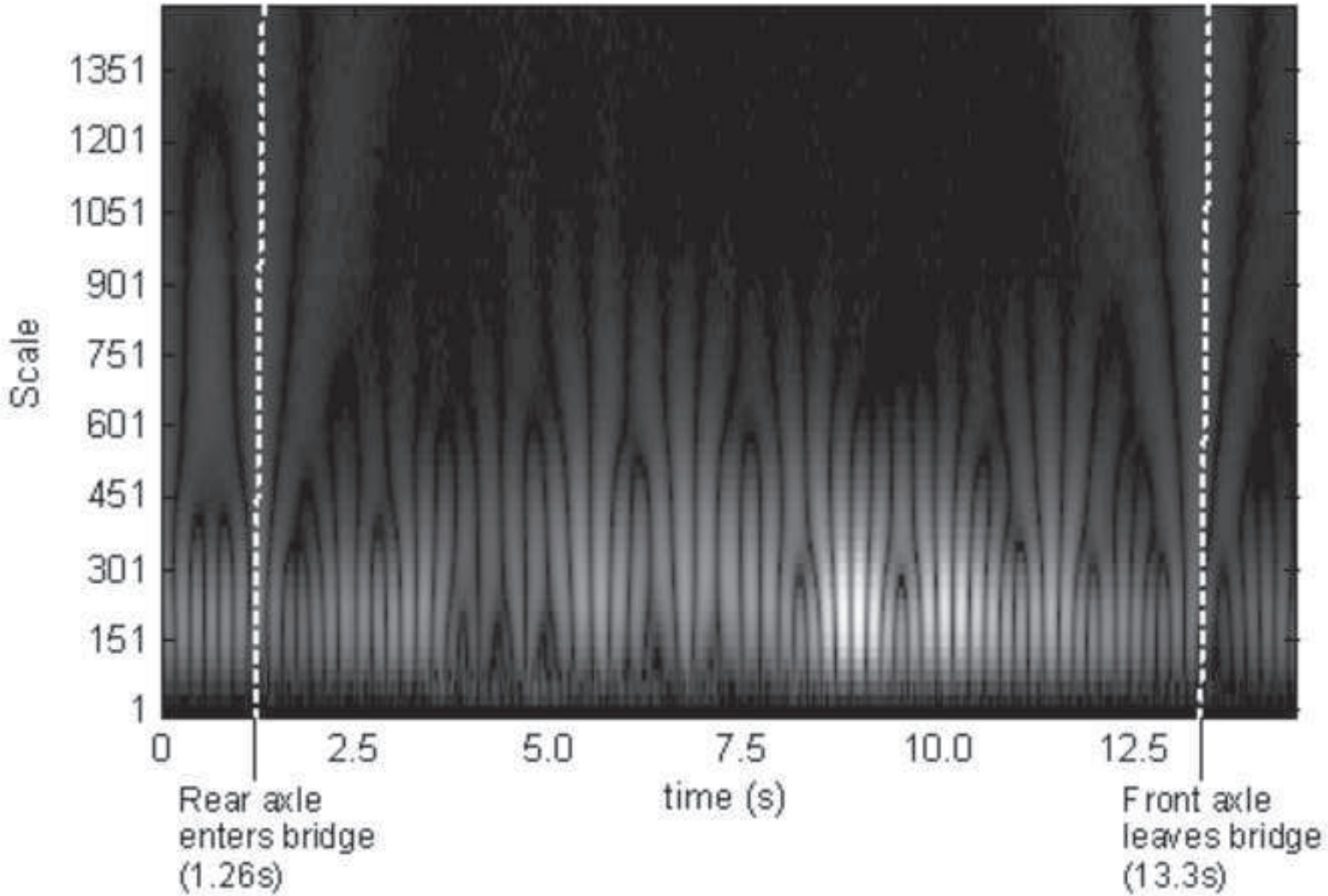

Figure 28
Click here to download high resolution image

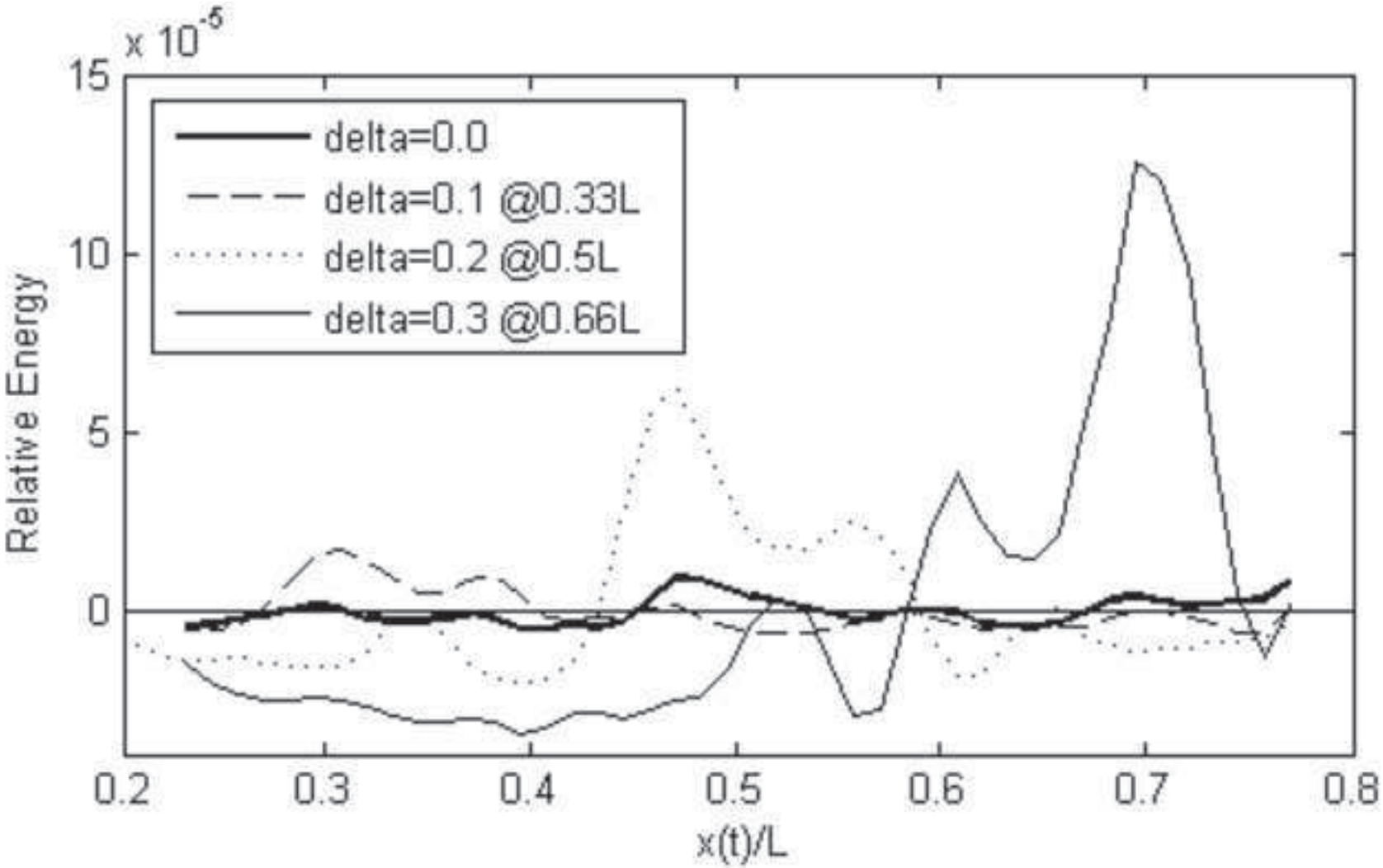

Figure 29
Click here to download high resolution image

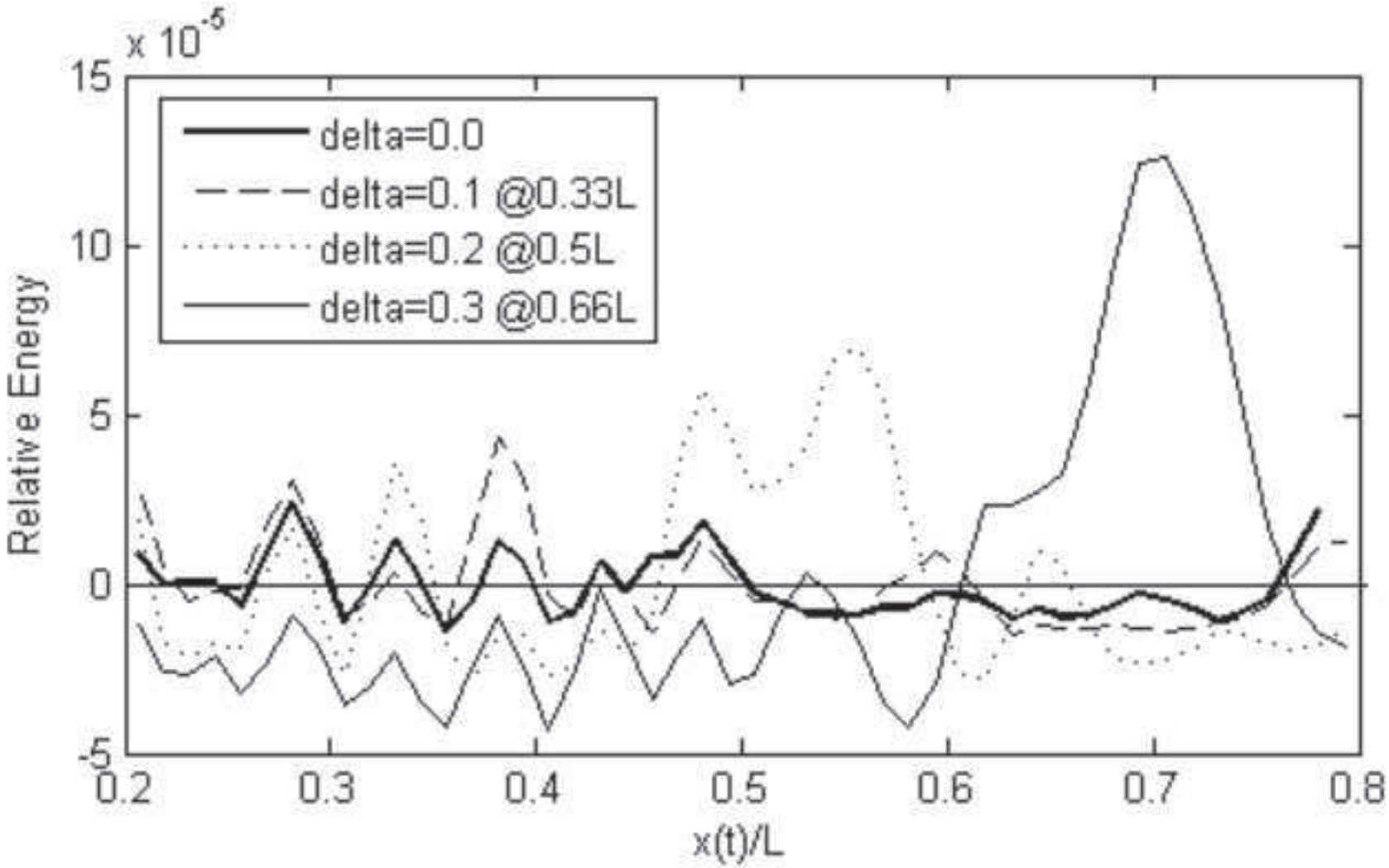

Figure 30
Click here to download high resolution image